https://doi.org/10.5194/egusphere-2024-2157
Preprint. Discussion started: 2 September 2024

Investigating ice formation pathways using a novel two-moment multi-class cloud microphysics scheme

Tim Lüttmer[1], Peter Spichtinger[1], and Axel Seifert[2]

[1]Institute for Atmospheric Physics, Johannes Gutenberg University Mainz, Mainz, Germany
[2]Deutscher Wetterdienst, Offenbach, Germany

Correspondence: Tim Lüttmer (tluettm@uni-mainz.de)

Abstract. We developed a novel microphysics scheme to investigate the formation pathways of ice crystals in the atmosphere. The new two-moment scheme distinguishes between five ice classes ('ice modes') each with their unique formation mechanism: homogeneous freezing of solution droplets, deposition nucleation, homogeneous freezing of cloud droplets and raindrops, immersion freezing and secondary ice from rime splintering. The ice modes interact with each other, e.g. in competition for growth by deposition of water vapor and aggregation, but also with the other cloud particle classes, i.e., cloud droplets, rain, snow, graupel, hail.

This scheme was employed to investigate the liquid origin vs in-situ formation in the fully glaciated parts of an idealised convective cloud. Liquid origin ice clouds stem from droplets that freeze close to water saturation. In-situ formed ice clouds form directly from the vapor phase below water saturation. The majority of the cloud ice in the deep convection cloud consisted of frozen droplets (liquid origin). This was caused by the high number concentration of cloud droplets available for freezing. In-situ formed ice was only relevant for the overshoot where ice from both formation pathways mixed.

The new scheme is also useful for investigation of the ice formation in the mixed-phase parts of the convective cloud. There is a vertical layering of ice modes in the cloud. The lower most layer consists of secondary ice from rime splintering and occurred near the updraft core at temperatures around the Hallet-Mossop zone. In an altitude between 6 and $9\,\mathrm{km}$ ice mostly stems from immersion freezing. We find a correlation between the abundance of ice from immersion freezing and snow. The majority of ice crystals above $9\,\mathrm{km}$ stems from homogeneously frozen cloud droplets since ice nucleating particles (INP) required for immersion freezing where quickly depleted.

1 Introduction

Clouds constitute an important but still quite uncertain component of the Earth-Atmosphere system. They influence the hydrological cycle (e.g. by forming precipitation) and also the system's energy budget by interaction with solar and thermal radiation. Incoming solar radiation is partly scattered and reflected back to space (albedo effect) whereas the Earth's outgoing infrared radiation is partly absorbed and re-emitted at a different temperature (greenhouse effect).

Clouds cover a large part of the planet and are thus omnipresent in the atmosphere. Nevertheless, our understanding of clouds and the relevant and dominant processes is still quite limited, especially for clouds containing ice particles. Here, we can dis-

https://doi.org/10.5194/egusphere-2024-2157
Preprint. Discussion started: 2 September 2024

criminate between two thermodynamic regimes. In the temperature regime $235\,\mathrm{K} \leq T \leq 273\,\mathrm{K}$ super-cooled liquid droplets as well as ice crystals can co-exist; clouds containing both kinds of hydrometeors are called mixed phase clouds. At lower temperatures, only the solid phase exists, i.e. we find pure ice clouds.

However, even for pure ice clouds at low temperatures, the pathway of formation remains unclear a priori. The different formation mechanisms were recently summarized and classified in the following ways [see, e.g., Krämer et al. (2016); Wernli et al. (2016)]:

- Formation pathways related to freezing of pre-existing cloud droplets (i.e. in the mixed-phase temperature regime and close to water saturation) are termed liquid origin formation.
- Formation pathways related to direct formation of ice crystals from vapor at (liquid or solid) aerosols at low temperatures and below water saturation are termed in situ formation.

It is quite difficult to determine the formation pathway of ice crystals. For measured ice particles with imaging techniques there are some hints that complex shapes and large particle sizes are most probable for liquid origin ice crystals, whereas in situ formed ice crystals remain small, and their shapes remain simple (quasi-spherical or columnar shapes). This can be explained by the available water vapor, which can be used for diffusional growth. At the mixed phase regime, more water vapor is available leading to larger and more complex shapes, whereas at low temperatures the amount of water vapor is very limited leading to small sized and simple shaped ice crystals. It also seems to be probable that liquid origin ice clouds consist of much more ice particles than in situ formed ice clouds. This can be explained by the formation process. Liquid origin ice particles stem from pre-existing cloud droplets; the number concentration of water droplets in liquid clouds is usually in the order of some hundreds of particles per cubic centimeter and thus much larger than the amount of available ice nuclei at low temperatures.

Although there are some indications that we might be able to use the particle's properties themselves for a classification of the formation pathways, such evaluations are just based on single cases of measurements together with trajectory calculations and have an inherit uncertainty, which cannot be quantified. Therefore, a complementary viewpoint from the modeling perspective is necessary in order to give a more rigorous insight into the different formation mechanism in cloud systems, especially in vertically extending systems as convective clouds or warm conveyor belts.

In this paper we introduce a novel bulk scheme, the ice modes scheme, that features several ice classes each with their unique formation process. Using multiple ice classes instead of a single one allows to explore and evaluate the importance and bulk properties of each ice formation mechanism for a variety of clouds types, even synoptic-scale systems like outflow regions of Warm Conveyor Belts. With these tools we can also investigate the cloud evolution and radiative properties of clouds. Additionally we can evaluate the sensitivity of different ice formation pathways and their parametrisations to environmental conditions e.g. thermodynamic variables and domain properties like spatial and temporal resolution. In a first application of the new model we evaluate the formation of ice clouds for an idealized test case of convection. Although it was always assumed that the anvil of a convective thunderstorm should be mainly formed by frozen cloud droplets transported upwards, it was not shown before. Using our newly developed ice modes schemes, we can investigate this statement quantitatively.

https://doi.org/10.5194/egusphere-2024-2157
Preprint. Discussion started: 2 September 2024

In Section 2 we will describe the model equations and relevant microphysical parametrisations affecting ice in the model and than present a idealised simulation of a convective cloud in Section 3. We compare our results with a reference simulation that uses the standard double-moment scheme of Seifert and Beheng (2006) and also demonstrate the capabilities of the new scheme to characterize the origin of cloud ice and impact of different nucleation parametrisations.

2 Model description

The basis for our model development is the double-moment scheme of Seifert and Beheng (2006) (SB hereafter). The original SB scheme distinguished between six classes of cloud particles: cloud droplets, rain, (cloud) ice, snow, graupel and hail. While the formulation for the liquid droplet's treatment in the model remains unchanged, we reformulate the ice microphysics, and also the interaction of ice and water particles in terms of collision processes. In the following the new scheme is described.

2.1 General settings

The model formulation relies on the usual approach of a bulk model with two (general) moments. Instead of computing the temporal and spatial evolution of a (maybe multivariate) mass distribution with a Boltzmann-type evolution equation, we use the integrated version, i.e., the evolution equations for moments of the underlying mass distribution of the respective class of hydrometeors. The moments are defined in the usual way, i.e.

$$M_i^k := \int_0^\infty x^k \, f_i(x) \mathrm{d}x \tag{1}$$

with the mass of particles x for the respective class i of hydrometeors. The mass distribution is normalized by the total number concentration of particles n_i. For a meaningful closure of the systems of equations, we have to choose a suitable type of mass distribution. We generally assume that the particle mass distributions can be represented by generalized Gamma-distributions (see also Seifert and Beheng, 2006) of the form

$$f_i(x) = A_i x^{\nu_i} \exp(-\lambda_i x^{\mu_i}) \tag{2}$$

where the shape parameters ν_i and μ_i are prescribed, λ_i and A_i are linked to the zeroth and first distribution moments, the number concentration n_i and the mass content q_i

$$n_i = M_i^0 = \int_0^\infty f(x) \, \mathrm{d}x = \frac{A}{\mu \lambda^{\frac{\nu+1}{\mu}}} \Gamma\left(\frac{\nu+1}{\mu}\right) \tag{3}$$

$$q_i = M_i^1 = \int_0^\infty f(x) x \, \mathrm{d}x = \frac{A}{\mu \lambda^{\frac{\nu+2}{\mu}}} \Gamma\left(\frac{\nu+2}{\mu}\right) \tag{4}$$

See Appendix B for details on the properties of the gamma distribution and the analytical solution of the integrals.

For the formulation of single particle processes (e.g. growth or sedimentation), we have to introduce size-mass relations and

https://doi.org/10.5194/egusphere-2024-2157
Preprint. Discussion started: 2 September 2024

velocity-mass relations of the form

$$D_i(x) = a_i x^{b_i}, \;\; v_i(x) = \alpha_i x^{\beta_i} \tag{5}$$

with the (generalized) size D_i and the terminal velocity v_i for a particle of mass x within a class i, respectively. These relations represent the different shapes of particles from different classes. The remaining classes of hydrometeors are labeled by indices, i.e. c for cloud droplets, r for rain drops, s for snow, g for graupel, and h for hail, respectively. The old class cloud ice is now splitted into five classes. For details of the formulation and the determination of the shapes for the used hydrometeor classes we refer to Seifert and Beheng (2006).

For our newly introduced ice modes we use the same parameters of the distribution (2) and the relations (5) for all classes. While the formation pathway of an ice crystal might have an impact on its shape, the morphology of the particle is mainly determined by the environmental conditions encountered during its growth, e.g., temperature and humidity (see, e.g., Magono and Lee, 1966; Kobayashi, 1967; Libbrecht, 2005; Pruppacher et al., 2010), which is not accounted for in the SB scheme. Using the same coefficients and parametrisations for each ice mode apart from its source also has the advantage that it allows a more concise interpretation on the impact of the individual ice formation pathways on the cloud evolution.

The time evolution of the kth-moment M_i^k of an ice mode i (or another class of hydrometeors) is governed by

$$\frac{\partial M_i^k}{\partial t} + \boldsymbol{\nabla} \cdot \left[\boldsymbol{v} M_i^k\right] + \frac{\partial \bar{v}_{i,k} M_i^k}{\partial z} - \boldsymbol{\nabla} \cdot \left[K_h \boldsymbol{\nabla} M_i^k\right] = \text{Source/Sink} \tag{6}$$

The terms on the left-hand side describe the effects of advection with the mean wind velocity $\boldsymbol{v}$, sedimentation with the weighted mean fall-speed $\bar{v}_{i,k}$ and turbulent mixing with the mean turbulent diffusivity of heat K_h, respectively. On the right-hand side are the source and sink terms for the particle formation, which is unique for each ice mode, deposition of water vapor and evaporation and a number of collisions processes, most importantly aggregation and riming, respectively. Actually, these equations must be coupled with a model for atmospheric flows, as, e.g., suitable approximations of the Navier-Stokes equations within the ICON model.

In the following we will focus on the description of the ice related physics and refer to Seifert and Beheng (2006) for an in-depth description of the warm- and mixed-phase microphysics.

2.2 Ice formation pathways

For the treatment of ice particles, we introduce new classes of ice particles, discriminated by their formation mechanisms. The ice modes scheme features five independent ice classes instead of a single one (former class “cloud ice”), called ice modes in this work, each with their unique formation pathway. For each new ice mode, we introduce number concentrations and mass content, respectively. The other classes (graupel, hail and snow) remain unchanged; however, we have to reformulate the processes of interactions between the former class “cloud ice” and other variables (e.g. for collision processes, see below). The new classes are as follows:

- Homogeneous freezing of cloud droplets n_{frz}, q_{frz}

https://doi.org/10.5194/egusphere-2024-2157
Preprint. Discussion started: 2 September 2024

- Immersion freezing of cloud and rain droplets n_{imm}, q_{imm}
- Freezing of solution droplets (homogeneous nucleation) n_{hom}, q_{hom}
- Deposition nucleation n_{dep}, q_{dep}
- Secondary ice from rime splintering n_{sec}, q_{sec}

The sum of all ice modes represent all ice crystals present (n_{tot}, q_{tot}).

2.2.1 Ice cloud classification due to formation pathway

The basis for the classification of ice clouds formation by different pathways is given by the thermodynamic properties of water. Liquid water is the stable phase at temperature above the triple point $T_m = 273.16\,\mathrm{K}$. Below this temperature, pure liquid water is meta stable, i.e., it can be supercooled down temperatures around $T \sim 235\,\mathrm{K}$; at lower temperatures, liquid droplets freeze almost instantaneously to form the stable phase in the regime $T < T_m$, i.e. the solid phase of hexagonal ice.

Ice formation is always triggered by the formation of a nucleation germ. The germ could either form spontaneously by fluctuations within the liquid phase as a small cluster of molecules, which is then growing to the stable ice phase. This type of ice formation is called homogeneous freezing or homogeneous nucleation, since only liquid phases are involved. On the other hand, the surface of a solid aerosol particle, so called ice nucleating particle (INP) can serve as an ice nucleus, triggering ice formation. This type of ice formation is called heterogeneous nucleation (since another phase is involved). We distinguish between two ice modes of heterogeneous nucleation: immersion freezing and deposition nucleation. Immersion freezing is the initiation of droplet freezing by an INP located inside the droplet (Vali et al., 2015). Deposition nucleation on the other hand describes the deposition of supersaturated water vapor directly onto the INP and following formation of an ice crystal (Vali et al., 2015). There is a huge variety of experimental studies investigating different substances about their ice nucleating properties. However, we lack of theoretical understanding of the different formation mechanisms on a molecular basis, thus until now it is still quite unclear why some substances are good INP and why some others not. For an overview we refer to Hoose and Möhler (2012).

While this kind of classification might be relevant for investigating ice formation in laboratory studies, it is not quite meaningful for investigations of clouds and cloud systems. Therefore we use a different classification, as introduced by Krämer et al. (2016); Wernli et al. (2016), which is more related to the usual description of clouds.

https://doi.org/10.5194/egusphere-2024-2157
Preprint. Discussion started: 2 September 2024

– Liquid origin: Once a cloud consisting of water particle has formed, it can only exist at or close water saturation. If these cloud droplets are cooled down below the triple point and freeze to ice particles, this pathway is called "liquid origin". Thermodynamically, the system is well characterized as close to water saturation (but supersaturated with respect to ice) and in the temperature range $235 \leq T \leq T_m$.

– In situ formation: If there are no pre-existing cloud particles available, in an environment which is supersaturated with respect to ice (but subsaturated with respect to water), ice particles can form either from aqueous solution droplets (i.e. liquid aerosol droplets) by spontaneous freezing or by deposition of water vapor on available solid aerosol particles (deposition nucleation). Both formations mechanisms are subsummed by the term in situ formation.

In regards to this classification scheme of ice clouds (liquid origin vs. in situ formation), homogeneous and deposition nucleation contributes to in-situ cirrus and homogeneous as well as immersion freezing of cloud droplets and rain to liquid origin cirrus. Ice particles formed by secondary ice production can not be attributed to either due to secondary ice production's intrinsic link to multiple other ice particle formation pathways, e.g., aggregation and riming.

2.2.2 Homogeneous freezing of cloud droplets

Cloud droplets are considered to be pure water droplets, thus freezing homogeneously at temperatures below the triple point T_m but at water saturation. Homogeneous freezing of cloud droplets is the source for the FRZ ice mode with the bulk quantities q_{frz} and n_{frz}. The stochastic process of homogeneous freezing is described by a nucleation rate J_{hom} ($\mathrm{m^{-3}s^{-1}}$), which depends on temperature only (since existence of cloud droplets requires water saturation), thus the change in number and mass concentrations of the ice mode can be described by

$$\frac{\partial n_{frz}}{\partial t} = J_{hom} q_c, \quad \frac{\partial q_{frz}}{\partial t} = J_{hom} q_c x_c \frac{\nu_c + 2}{\nu_c + 1} \tag{7}$$

using the mass mixing ratio of cloud droplets q_c, the mean mass of cloud droplets x_c and the distribution shape parameter ν_c of the cloud mass distribution (generalized gamma distribution), respectively. For the formulation of the homogeneous freezing coefficient of cloud droplets in $\mu\mathrm{kg^{-1}s^{-1}}$, we use the fit of Cotton and Field (2002) to the formulation of Jeffery and Austin (1997):

$$\log\left(\frac{J_{hom}}{\rho_w}\right) = \begin{cases} -243.4 - 14.75T - 0.307T^2 - 0.00287T^3 - 1.02 \cdot 10^{-5}T^4 & \text{for} T \leq -30\,^\circ\mathrm{C} \\ -7.63 - 2.996(T + 30) & \text{for} T > -30\,^\circ\mathrm{C} \end{cases} \tag{8}$$

whereas ρ_w denotes the liquid water density. The direct numerical integration is possible since due to saturation adjustment for the cloud droplets (see SB), the system stays at water saturation permanently.
Homogeneous freezing of raindrops in the SB scheme is omitted, since raindrops freeze rapidly by heterogeneous freezing before reaching temperature levels close to the homogeneous freezing temperature.

https://doi.org/10.5194/egusphere-2024-2157
Preprint. Discussion started: 2 September 2024

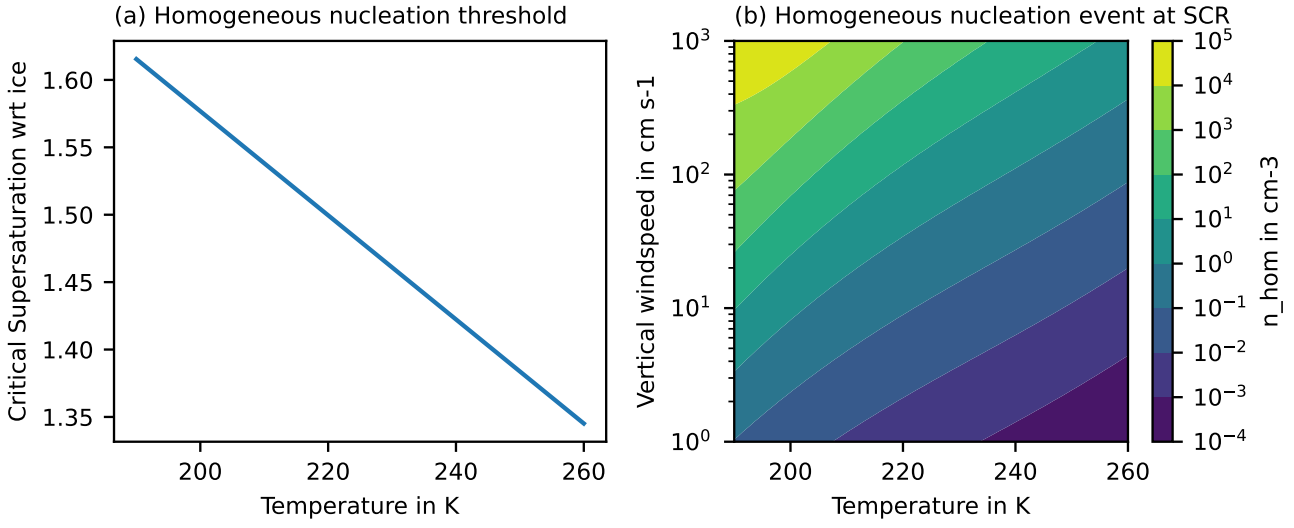

Figure 1. Homogeneous nucleation following Kärcher et al. (2006) for no pre-existing ice. (a) Critical supersaturation serves as a nucleation threshold and (b) number of ice crystals after an homogeneous nucleation event at S_{cr}.

2.2.3 Homogeneous freezing of solution droplets

Aequeous solution droplets, i.e. liquid aerosol particles can be supercooled to lower temperatures than pure liquid droplets. The solute obviously impedes the establishment of a critical cluster. Koop et al. (2000) showed that the effect of solutes on the freezing temperature is driven by their thermodynamic (equilibrium) quantities, which can be expressed in terms of water activity, that is defined as the water saturation vapor pressure ratio between the solution and pure water $a_w = e_{sol}/e_{liq}$. When we assume that the solution droplet is in a thermodynamic equilibrium with its environment than the freezing temperature is independent of the choice of chemical droplet composition, at least for inorganic compounds. This translates into a nucleation rate for solution droplets, which solely depends on the environmental conditions, i.e. temperature and supersaturation with respect to ice, but not on the substance in the water drops. The nucleation rate can be formulated using a threshold of critical supersaturation, as could be shown by Spichtinger et al. (2023), e.g., using the formulation by Ren and MacKenzie (2005)

$$S_{\text{cr}} = 2.349 - T/259. \tag{9}$$

Panel (a) in Figure 1 shows that quite high supersaturations ($S_i > 1.4$) are necessary for homogeneous nucleation events to occur, especially in low temperature regimes ($T < 230\,\text{K}$) where freezing of pure water droplets is no longer possible and homogeneous nucleation commonly observed. This ice formation process is called homogeneous nucleation and the source term for the HOM ice mode with the bulk properties n_{hom} and q_{hom}. Generally, we would obtain similar equations for the change in n, q as for the freezing of cloud droplets (see Section 2.2.2). However, since the system is in a non-equilibrium state and there is no boundary condition (like the assumption of water saturation as above), we would have to represent the evolution

https://doi.org/10.5194/egusphere-2024-2157
Preprint. Discussion started: 2 September 2024

of the saturation ratio, changed also by diffusional growth; this would require a small timestep for the numerical scheme and thus is not feasible.

Therefore, we use the parameterisation by Kärcher and Lohmann (2002), which describes the homogeneous nucleation event in an ascending air parcel. When an air parcel ascends adiabatically supersaturation is generated by adiabatic cooling. When the critical supersaturation S_{cr} is reached, homogeneous nucleation is triggered. The newly nucleated ice crystals deplete supersaturation by depositional growth. The competition between generating supersaturation by adiabatic cooling and depleting supersaturation by depositional growth in a adiabatically ascending air parcel, driven by a constant wind velocity w can be described as

$$\frac{dS}{dt} = a_1 S w - (a_2 + a_3 S) R_i(t) \tag{10}$$

with the parameters

$$a_1 = \frac{L_s M_w g}{c_p R T^2} - \frac{M_a g}{RT},\ a_2 = \frac{T k_b}{e_{sat,i}},\ a_3 = \frac{L_s^2 M_w m_w}{c_p p T M_a} \tag{11}$$

a_1 describes the effect of adiabatic cooling, where a_2, a_3 and R_i describe the depletion of supersaturation by depositional growth as a function of time. The parameters and process of depositional growth will be further explained in Section 2.3.

If the air parcels continues to rise, aqueous solution droplets continue too freeze. When the newly nucleated ice crystals deplete more supersaturation than is being generated by adiabatic cooling, the maximum value of the supersaturation S_* is reached. The supersaturation is depleted and once it reaches S_{cr} the freezing of solution droplets stops. The integrated number of solution droplets frozen within the freezing time interval t_* described the number of ice crystals from the homogeneous nucleation event. Numerical simulations suggest that the freezing time interval t_* is short and the maximum value of supersaturation S_* is approximately equal to S_{cr} (Kärcher et al., 2006). Thus the number concentration of ice particles in a homogeneous nucleation event can than be estimated as

$$n_{hom} = w \frac{a_1 S_{\text{cr}}}{a_2 + a_3 S_{\text{cr}}} \frac{1}{R_{im}(r_0)} \tag{12}$$

R_{im} is the analytical approximation of the integral that describes the growth of the solution droplet within the freezing time interval where we refer to Kärcher et al. (2006) for a detailed derivation. $r_0 = 27.2\,\text{nm}$ is the radius of the monodisperse aqueous solution droplets. We obtain the bulk mass of the newly nucleated homogeneous ice mode as

$$q_{hom} = \frac{4}{3}\pi\rho_i \left(\frac{r_0(1 + b_{KH} r_0) - 1}{b_{KH}} \right)^3 n_{hom} \tag{13}$$

with the parameter $b_{KH} = \frac{\alpha_d v_{th}}{4 D_v}$. α_d is the deposition coefficient, v_{th} is the mean molecular velocity of water vapor, and D_v denotes the diffusivity.

Panel (b) in Figure 1 shows the number concentration of ice n_i after a homogeneous nucleation event at critical supersaturation S_{cr} for vertical windspeeds ranging from synoptic velocities (up to $10\,\text{cms}^{-1}$), gravity waves (up to $100\,\text{cms}^{-1}$) and convection (up to $1000\,\text{cms}^{-1}$). Homogeneous nucleation is strongly sensitive to the model level vertical windspeed and large nucleation events can only be represented if vertical windspeeds are resolved, and no other nucleation mechanisms disturbs the

https://doi.org/10.5194/egusphere-2024-2157
Preprint. Discussion started: 2 September 2024

effect of homogeneous nucleation. Nucleation events at synoptic vertical windspeed will be more common in the model and nucleate up to $1\,\mathrm{cm}^{-3}$ ice crystals. Note that the parametrisation of Kärcher et al. (2006) does not explicitly scale with the microphysics time step as it describes an entire nucleation event and not a nucleation rate. Shorter time steps might lead to higher number concentrations because newly nucleated ice crystals have less time to deplete the supersaturation until a new event is allowed to trigger. However, the homogeneous ice mass content is still constrained by the the availability of supersaturation, i.e. by thermodynamics.

The ice modes scheme uses the extension of Kärcher et al. (2006) where the effect of pre-existing ice depleting supersaturation is taken into account as an equivalent to a fictitious downdraft velocity w_{pre}

$$w' = w - w_{pre} = w - \frac{a_2 + a_3 S_i}{a_1 S_i} R_{i,pre} \tag{14}$$

with w as the model level vertical wind speed and $R_{i,pre}$ as the mean radius of the pre-existing ice. Pre-existing ice usually originates from a heterogeneous ice mode or a prior homogeneous nucleation event, as we will see in our simulation results.

2.2.4 Heterogeneous nucleation

In the new scheme we use the two nucleation pathways, i.e. immersion freezing and deposition nucleation. Both ice formation pathways depend on temperature, supersaturation and properties of the INP like effectiveness and number of sites causing nucleation per unit surface area (Vali et al., 2015). Both immersion freezing of raindrops and cloud droplets are considered in this model.

We obtain the number density for the immersion freezing ice mode as the sum of freezing cloud and rain droplets as

$$\frac{\partial n_{imm}}{\partial t} = C_{IMM}|_c - n_{inact} + \frac{\partial n_{imm}}{\partial t}|_r \tag{15}$$

and the mass density as

$$\frac{\partial q_{imm}}{\partial t} = \frac{\partial n_{imm}}{\partial t}|_c x_c + \frac{\partial q_{imm}}{\partial t}|_r \tag{16}$$

with the mean cloud droplet mass x_c. Similarly we obtain for the number density of the deposition nucleation ice mode

$$\frac{\partial n_{dep}}{\partial t} = C_{DEP} - n_{inact} \tag{17}$$

and the mass density

$$\frac{\partial q_{dep}}{\partial t} = \frac{\partial n_{dep}}{\partial t} x_{i,min} \tag{18}$$

with the minimum mass of ice crystals in the model $x_{i,min}$. C_{IMM} and C_{DEP} describe the number concentration (m^{-3}) of activated INPs for immersion freezing (of cloud droplets) and deposition nucleation, respectively. The model does not feature an explicit model for INP or aerosols in general. Instead the number of activated INPs n_{inact} (m^{-3}) is tracked and advected along with the other ice bulk properties. In further nucleation events n_{inact} is subtracted from the INP number. n_{inact} relaxes

https://doi.org/10.5194/egusphere-2024-2157
Preprint. Discussion started: 2 September 2024

back to zero in an ice free environment.

$$\frac{\partial n_{inact}}{\partial t} = \begin{cases} -\frac{n_{inact}}{\tau_{inact}} & \text{if } q_{tot} = \frac{\partial n_{imm}}{\partial t} = \frac{\partial n_{dep}}{\partial t} = 0 \\ \frac{\partial n_{imm}}{\partial t} + \frac{\partial n_{dep}}{\partial t} & \text{else} \end{cases} \tag{19}$$

with the relaxation time scale $\tau_{inact} = 600\,\mathrm{s}$ and the total ice content (as the sum of all ice modes) q_{tot}.

First, we describe immersion freezing for rain droplets, i.e. for large water droplets. Bigg (1953) performed laboratory studies investigating the freezing of supercooled purified water in the presence of INP and estimated the probability of a raindrop freezing depending on temperature and droplet volume. Using this results the freezing rate of rain can be expressed as

$$\frac{\partial n_{imm}}{\partial t}|_r = -J_{bigg} q_r = -A_{imm} \rho_w^{-1} \exp(B_{imm}(T_m - T) - 1) q_r \tag{20}$$

where we use the coefficients $A_{imm} = 200\,\mathrm{m^{-3}s^{-1}}$ and $B_{imm} = 0.65\,\mathrm{K^{-1}}$ for rain water due to Barklie and Gokhale (1959). We obtain the mass of frozen raindrops as

$$\frac{\partial q_{imm}}{\partial t}|_r = -A_{imm} \rho_w^{-1} \exp(B_{imm}(T_m - T) - 1) q_r x_r Z_r \tag{21}$$

with the second moment of the rain mass distribution $Z_r = M_r^2$ and the melting temperature T_m. The mass and number density of frozen raindrops is partitioned into the immersion freezing ice mode (IMM), graupel and hail depending on its diameter. Raindrops smaller than $0.5\,\mathrm{mm}$ freeze into ice, raindrops with sizes between $0.5\,\mathrm{mm}$ and $1.25\,\mathrm{mm}$ are shifted into the graupel class, and raindrops larger than $1.25\,\mathrm{mm}$ are considered as hail.

Second, we present the nucleation schemes for immersion freezing of cloud droplets and deposition nucleation, respectively, resulting into changes in the ice modes n_{imm}, q_{imm} (immersion freezing) and n_{dep}, q_{dep} (deposition nucleation).

The ice mode scheme offers the choice between the three heterogeneous nucleation schemes, i.e. Hande et al. (2015), Ullrich et al. (2017), Phillips et al. (2008). Hande et al. (2015) (HA15) considered dust as the main source for INPs over Europe. They used the COnsortium for Small-scale MOdelling (COSMO) meteorological model coupled to the MUlti-Scale Chemistry Aerosol Transport (MUSCAT) to simulate Sahara dust outbreaks for the year 2008. From the statistics of simulated dust concentrations HA15 calculated atmospheric profiles of potential INPs. Since Sahara dust outbreaks shows a strong seasonal variability HA15 provided mean profiles for each season. The number of active INPs for immersion freezing was than parameterised using the laboratory results of Niemand et al. (2012) for dust particles

$$C_{IMM}(T) = A_H \cdot \exp\left[-B_H (T - T_{H,min})^{C_H}\right] \tag{22}$$

valid for the temperature range from $T_{H,min} = 237.15\,\mathrm{K}$ to $261.15\,\mathrm{K}$ with the set of coefficients $A_H, B_H, C_H, T_{H,min}$ being chosen depending on the season (see Table 1 in Hande et al. (2015)). The number concentration of active INPs for deposition nucleation was estimated using the parametrisation of Steinke et al. (2015)

$$C_{DEP}(T, S_i) = C_{IMM}(T) \cdot (a_H \arctan(b_H(-100) + c_H) + d_H) \tag{23}$$

for temperatures between $T_{H,min} = 220\,\mathrm{K}$ and $253\,\mathrm{K}$. Again, the coefficients depend on the season (see Table 1 in Hande et al. (2015)).

https://doi.org/10.5194/egusphere-2024-2157
Preprint. Discussion started: 2 September 2024

Ullrich et al. (2017) (UL17) used 11 years of data from ice nucleation experiments in the Aerosol Interaction and Dynamics in the Atmosphere (AIDA) cloud chamber to develop a empirical parametrisation for both immersion freezing and deposition nucleation. Dust and soot samples of different types, collected in various locations of the world were analysed in AIDA. The data set includes the results published in Niemand et al. (2012), which where also used in the HA15 parametrisation. However, their are some differences in their approach to calculate the density of active surfaces sites (see Ullrich et al. (2017)) resulting in a light shift to higher densities. In this study we only consider the dust mode. We obtain the number of active INP for immersion freezing and deposition nucleation, respectively, for dust by

$$C_{IMM/DEP}(T,S_i) = n_a\left(1-\exp\left[-n_{s,IMM/DEP}(T,S_i)SA_a\right]\right) \tag{24}$$

with the aerosol number concentration n_a (m^{-3}), the aerosol surface area concentration SA_a and the ice nucleating active surface site density $n_{s,IMM/DEP}$ (m^{-2}) for immersion freezing and deposition nucleation, respectively. The ice nucleating active surface site density for immersion freezing follows a simple exponential temperature profile

$$n_{s,IMM} = \exp[150.577 - 0.517T] \tag{25}$$

and for deposition nucleation

$$n_{s,DEP} = \exp\left[\alpha(S_i-1)^{1/4}\cos(\beta(T-\gamma))^2\operatorname{arccot}(\kappa(T-\lambda))\right] \tag{26}$$

where the fixed coefficients α, β, γ, κ and λ can be found in Ullrich et al. (2017). For dust size distribution we use a sum of three lognormal distribution modes. The distribution parameters were chosen such that the immersion freezing temperature profile for UL17 is similar to HA15.

Phillips et al. (2008) (PH08) developed a empirically derived framework for heterogeneous nucleation of multiple aerosol species.

INP are grouped into three basic types: dust/metallic aerosols, inorganic black carbon and insoluble biological aerosol like bacteria and pollen. The basic assumption is that the ice nucleating activity of insoluble aerosol depends on its number of sites causing nucleation (active sites) and hence is proportional to the total aerosol surface area. The number concentration of active INP for a aerosol group X was parameterised as

$$C_{INP,X} = \int_{D_{X,min}}^{\infty} (1-\exp[-\mu_X(D_X,T,S_i)])f_X(D_X)\,\mathrm{d}D_X \tag{27}$$

where μ_X is the Poisson distributed average of the number of activated INPs for each aerosol particle of size D_X. μ_X was empirically determined by using observational and laboratory data (Phillips et al., 2008). The ice mode schemes uses a simple lookup table and 2D interpolation to determine the fraction of activated INPs as function of temperature and supersaturation for each aerosol type. Lognormal size distributions are assumed for all aerosol types. The number of INPs is the sum over all three aerosol types with the associated number concentration n_X and active fraction $C_{INP,X}$

$$C_{INP} = \sum_X C_{INP,X}(T,S_i)n_X \tag{28}$$

https://doi.org/10.5194/egusphere-2024-2157
Preprint. Discussion started: 2 September 2024

where we obtain the number of INPs for immersion freezing at and for deposition nucleation below saturation wrt to water. The initial number concentration of soot particles and biological aerosol is fixed and the number concentration of dust varies with altitude z following a prescribed background profile

$$n_{\text{dust}}(z) = n_{\text{dust},0} \exp\left[\frac{z_{\text{dust},0} - z}{z_{\text{dust},e}}\right] \tag{29}$$

Unless otherwise noted we only consider the dust mode for PH08 in this work. We chose $z_{\text{dust},0}$ such that the maximum number of INPs activated for immersion freezing is the same as for HA15.

Panel (a) in Figure 2 shows the temperature profiles for immersion freezing parametrisations (IMM) and contour plots of deposition nucleation (c-d). PH08 uses geometric altitude as a coordinate for dust concentration. We transform the altitude into a temperature coordinate using the ICAO Standard Atmosphere. The profile labeled PH08+ considers also soot and biological aerosols in addition to dust. The exponential profiles of immersion freezing for HA15 and UL17 are very similar starting both close to 260 K and being capped at the homogeneous freezing temperature threshold. It is not surprising that we only observe minor differences since INP activation in both parametrisations is based on mostly the same laboratory studies. On the other hand immersion freezing for PH08 starts a higher temperatures but increases less steeply past 260 K. For convectively driven clouds this means an earlier onset of ice formation and has potentially strong effects on the evolution of the ice phase in mixed-phase clouds. PH08+ shows activation of INP at even higher temperature caused by soot and biological aerosol. However, since we did not tune this version of the PH08 scheme to HA15 the maximum number of active INP is lower.

2.2.5 Secondary ice production

Supercooled droplets colliding with ice particles (riming), especially graupel and hail, can throw off small ice splinters, which can grow into ice crystals. This phenomenon was first investigated by Macklin (1960). Various physical mechanism have since been suggested: Macklin (1960) reported that riming caused the growth of fine ice structures that would break to create secondary ice splinters while Choularton et al. (1978) suggested that shattering of freezing droplets produces the ice splinters. Hallett and Mossop (1974) counted ice crystals in a light-beam beneath a metal rod, which moved through the cloud chamber and sweeped up water droplets causing riming. By comparing the enhanced number of ice crystals to the background number of the cloud chamber they derived a profile depending on cloud temperature. The standard parametrisation for RS is based on this study and often referred to as the the Hallett-Mossop process.

Emersic and Connolly (2017) investigated riming events using high-speed cameras concluded that even small ice crystals and not only large rimers like graupel could potentially produce a significant amount of secondary ice fragments. Seidel et al. (2024) investigated rime splintering with high-speed video microscopy, IR thermography and a custom-build ice counter. They could not reproduce the results of Hallett and Mossop (1974). In general they found only insignificant amounts of SIP production during riming, which can not explain the amount of SIP expected in convective and frontal clouds.

Overall Korolev and Leisner (2020) found no consistency in measured or estimated rime splintering rates between various groups and attributed the discrepancy to different laboratory setups and techniques. Despite RS being the most commonly included secondary ice mechanism in numerical cloud models, the physical understanding is severely lacking and thus the

https://doi.org/10.5194/egusphere-2024-2157
Preprint. Discussion started: 2 September 2024

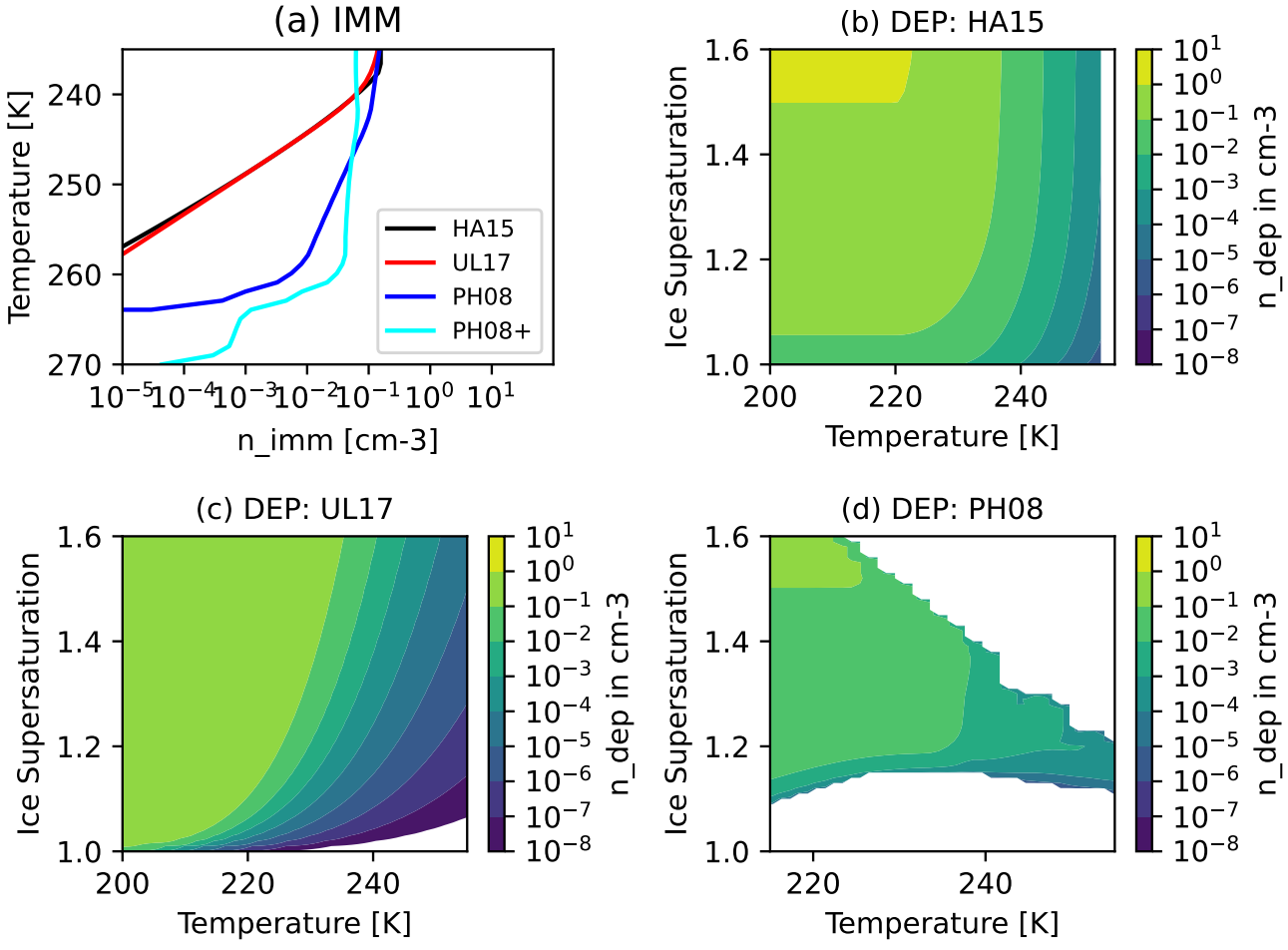

Figure 2. Number concentration of activated INPs for (a) Immersion freezing with profiles for HA15, UL17, PH08 and PH08+ schemes and (b-d) deposition nucleation as a function of T and S_i for (b) HA15, (c) UL17, (d) PH08.

development of a physically based parameterisation seems unfeasible at the moment (Korolev and Leisner, 2020). Still we will use the parameterisation of RS based on the dataset of Hallett-Mossop extensively in this work as it part of the standard SB scheme.

In Hallett and Mossop (1974) rime splintering occurred within a narrow temperature range of $T_{rs,min} = 265\,\mathrm{K}$ and $T_{rs,max} = 270\,\mathrm{K}$. A fit onto their dataset is used as a function of temperature and rimed mass q_{rime} (kg) as it is implemented in SB

$$\frac{\partial n_{sec}}{\partial t} = q_{rime} C_{RS} \frac{T - T_{rs,min}}{T_{rs,opt} - T_{rs,min}} \frac{T - T_{rs,max}}{T_{rs,opt} - T_{rs,max}}$$
$$\frac{\partial q_{sec}}{\partial t} = \frac{\partial n_{sec}}{\partial t} x_{i,min} \tag{30}$$

https://doi.org/10.5194/egusphere-2024-2157
Preprint. Discussion started: 2 September 2024

with the multiplication factor $C_{RS} = 3.5 \cdot 10^8\,\mathrm{kg}^{-1}$ as well as the optimal temperature $T_{rs,opt} = 268\,\mathrm{K}$, the minimum temperature $T_{rs,min} = 265\,\mathrm{K}$ and the maximum temperature for splintering $T_{rs,max} = 270\,\mathrm{K}$. The triangular profile is centered at $T_{rs,opt}$ and ejects up to 350 splinters per mg rimed ice mass. The fragments are initialized as ice splinters of the minimum ice mass $x_{i,min} = 10^{-12}\,\mathrm{kg}$. Additional sources for secondary ice fragments from raindrop freezing and shattering as well as collisional breakup will be presented in another study.

2.3 Depositional growth of water particles

Deposition of water vapor onto a cloud particle in a supersaturated environment is the most fundamental growth process for all cloud particles. The SB scheme uses saturation adjustment for the water phase, hence whenever the environment is supersaturated wrt water ($S_w > 1$) at the beginning of a mircophysical time step, S_w is relaxed to water saturation (i.e. $S_w \equiv 1$) and the change of water vapor q_v is converted to cloud water q_c, considering latent heat release (using a Newton-Raphson scheme). However, supersaturation wrt ice (i.e. $S_i > 1$) is explicitly resolved. The mass growth of an ice particle by deposition of water vapor can be described by formulating the flux of vapor and heat between the particle and the environment considering mass and energy conservation, than integrating this fluxes over the particle surface and evaluating the effect of latent heat of sublimation on the particle surface temperature. Assuming that the temperature difference between the particle surface and the environment is small we can derive the general growth equation of a single ice particle with mass x using the Clausius-Clapeyron relation (Pruppacher and Klett, 1998)

$$\left.\frac{\partial x}{\partial t}\right|_{dep} = \frac{4\pi C(x)(S_i - 1)F_v(x)}{\frac{TR_v}{D_v e_{si}} + \frac{L_s\left(\frac{L_s}{R_v T} - 1\right)}{K_a T}} \tag{31}$$

with the saturation ratio wrt to ice $S_i = \frac{e}{e_{si}(T)}$, the ventilation coefficient F_v and the capacitance C accounting for the enhancement of the depositional growth by the flow field and the non-spherical shape, respectively. The left term in denominator represents the mass flux relation with the diffusion coefficient D_v and water vapor saturation pressure wrt ice $e_{si}(T)$; the right term describes the heat flux with the thermal conductivity of air K_a and the latent heat of sublimation L_s. The capacitance can be related to the maximum diameter $C(x) = D(x)/c$ with c_k depending on the class of the particle k.

Integrating (31) over the entire particle distribution for an ice mode k we obtain

$$\begin{aligned} g_{dep,k} &= \left.\frac{\partial q_k}{\partial t}\right|_{dep} = \int_0^\infty \left.\frac{\partial x_k}{\partial t}\right|_{dep} \mathrm{d}x_k \\ &= \frac{4\pi(S_i - 1)c_k^{-1}}{\frac{TR_v}{D_v e_{si}} + \frac{L_s\left(\frac{L_s}{R_v T} - 1\right)}{K_a T}} \int_0^\infty D(x_k) F_v(x_k) f(x_k)\,\mathrm{d}x_k \\ &= \frac{4\pi(S_i - 1)c_k^{-1}}{\frac{TR_v}{D_v e_{si}} + \frac{L_s\left(\frac{L_s}{R_v T} - 1\right)}{K_a T}} D(x_k) F_v \end{aligned} \tag{32}$$

with the mean particle mass x_k and averaged ventilation coefficient F_v; for details, see calculations in the Appendix of SB.

However, we must consider that all ice particle classes compete for water vapor. Thus we follow Morrison et al. (2005) semi-

https://doi.org/10.5194/egusphere-2024-2157
Preprint. Discussion started: 2 September 2024

analytic approach to estimate the depositional growth rate with a exponential relaxation towards equilibrium. The change of mass density of ice particle class k within a physical time step is

$$\left.\frac{\Delta q_k}{\Delta t}\right|_{dep} = \frac{\delta_i X}{\tau_k}\left(1-\exp\left(-\frac{\Delta t}{X}\right)\right) \tag{33}$$

with $\delta_i = q_v - q_{si}$ expressing the supersaturation wrt ice and the microphysical time step Δt. τ_k is defined as the depositional time scale

$$\tau_k^{-1} = \frac{g_{dep,k}}{\delta_i} \tag{34}$$

X is the conjoined relaxation time needed to describe the competition between the ice particle classes as a sum of the individual relaxation time scales

$$X = \left[\sum_j^N \tau_j^{-1}\right]^{-1} \tag{35}$$

where we consider graupel, hail, snow as well as all five ice modes. For a derivation and application of this method to resolve supersaturation see, e.g., Khvorostyanov (1995), Morrison et al. (2005), Köhler and Seifert (2015).

2.4 Sedimentation of cloud particles

For the sedimentation of ice particles, we use the mass-velocity relation (5) for ice crystals; these relations were used for all new ice modes. For the use in the evolution equation of moments (6), an averaged sedimentation velocity must be calculated via a weighted integration, i.e.

$$\bar{v}_{i,k} = \frac{1}{M_i^k}\int_0^\infty x^k f_i(x) v_i(x) \mathrm{d}x \tag{36}$$

Using the analytical results for generalized gamma-distributions, this results into the expression

$$\bar{v}_{i,k} = \alpha_i \frac{\Gamma\left(\frac{k+\nu_i+\beta_i+1}{\mu_i}\right)}{\Gamma\left(\frac{k+\nu_i+1}{\mu_i}\right)}\left[\frac{\Gamma\left(\frac{\nu_i+1}{\mu_i}\right)}{\Gamma\left(\frac{\nu_i+2}{\mu_i}\right)}\right]^{\beta_i} \bar{x}_i^{\beta_i} \tag{37}$$

see also Section 3.7 in SB.

2.5 Collision processes of cloud particles

Collision is an important process for producing large cloud particles. For the formation of large raindrops, collision is essential. However, considering the formation of rain via the ice phase, again collisions between water and ice particles play an important role. In the presented scheme, the rates for collisions between liquid particles (cloud droplets and raindrops) remain unchanged. However, the collision rates for ice particles must be reconsidered.

As formulated in the SB scheme, we have the following conceptual treatment for sorting new particles stemming from the collision of ice particles with others:

https://doi.org/10.5194/egusphere-2024-2157
Preprint. Discussion started: 2 September 2024

- Collision between an cloud ice particle and a cloud droplet leads to a larger ice particle or to a graupel particle, depending on the size of the ice particle (riming)
- Collision between two cloud ice particles leads to a snow particle (self-aggregation)
- Collision between an cloud ice particle and a snow particle leads to a snow particle (aggregation)

This concept must be adapted for ice particles from the five different ice modes. Especially, the collision of ice particles from different ice modes must be taken into account as a new process, extending the existing formulation of self-aggregation of ice particles. In the following the changes are documented.

2.5.1 Collision of liquid and solid particles

We adapt the formulation by SB of riming (ice particle collides with cloud droplet or raindrop) for all new ice modes. Analog to the implementation for a single ice class in SB, all ice modes can be collected by graupel, hail or snow and contribute to riming.

2.5.2 Aggregation of ice particles

There is no separate treatment for each ice mode regarding aggregation, all collisions between ice modes as well as self collection within a single ice mode contribute to the same snow class. The collision processes between two ice classes i and j leads to the formation of snow s can be described as

$$\left.\frac{\partial f_i(x)}{\partial t}\right|_{coll,ij} = -\int_0^\infty f_i(x) f_j(x') K_{ij}(x,x')\,\mathrm{d}x' \tag{38}$$

$$\left.\frac{\partial f_j(x)}{\partial t}\right|_{coll,ij} = -\int_0^\infty f_i(x') f_j(x) K_{ij}(x,x')\,\mathrm{d}x' \tag{39}$$

$$\left.\frac{\partial f_s(x)}{\partial t}\right|_{coll,ij} = \int_0^x f_i(x') f_j(x-x') K_{ij}(x',x-x')(x-x')\,\mathrm{d}x' \tag{40}$$

The collection kernel is defined as

$$K_{ij}(x_i,x_j) = A_{ij} E_{coll} |v_i(x_i) - v_j(x_j)| \tag{41}$$

where A_{ij} is the cross section of the sweep out volume, E_{coll} is the mean sticking efficiency and $v_{i,j}$ are the terminal velocities. Let D_i and D_j donate the maximum diameters of ice crystals and we obtain for A_{ij}

$$A_{ij}(x_i,x_j) = \frac{\pi}{4}(D_i(x_i) + D_j(x_j))^2 \tag{42}$$

https://doi.org/10.5194/egusphere-2024-2157
Preprint. Discussion started: 2 September 2024

where we simplified the expression by assuming spherical particles. The sticking efficiency is parameterised following Cotton et al. (1986)

$$E_{coll} = \min\left(10^{0.035\cdot(T-T_m)-0.7}, 0.2\right) \tag{43}$$

with a maximum efficiency of 0.2 for $T = 273\,\mathrm{K}$. The mass relation provided in equation (5) is not sufficient to characterise the terminal velocity of ice particles since complex shapes and atmospheric turbulence affect the flow field around the particle (Seifert, 2002). The velocity distribution function describes the probability of a ice particle of mass x to have the terminal velocity v'

$$P(v'|x) = \frac{1}{\sigma_{vel}\sqrt{2\pi}} \exp\left[-\frac{1}{2}\left[\frac{v' - v(x)}{\sigma_{vel}}\right]^2\right] \tag{44}$$

with the variance of terminal velocity σ_{vel}.

The absolute velocity difference in the collision kernel would split the integral and impose incomplete gamma functions thus complicating the result. We use the Wisner approximation which assumes characteristic mean values for the terminal velocities that are constant and can hence be separated from the integrand. As proposed in Seifert (2002) integral cross-section is used as a weight

$$\begin{aligned} {v_{ij,k}}^2 &= \frac{1}{N_k} \int_{x_i=0}^{\infty} \int_{x_j=0}^{\infty} D_i^2(x_i) D_j^2(x_j) f_i(x_i) f_j(x_j) x_i^k \\ &\int_{v_j=-\infty}^{\infty} \int_{v_i=-\infty}^{\infty} \left(v_i'(x_i) - v_j'(x_j)\right)^2 P(v_i'|x_i) P\left(v_j'|x_j\right) \mathrm{d}x_i \mathrm{d}x_j \mathrm{d}v_i' \mathrm{d}v_j' \\ &= v_i^2 \vartheta_i^k + v_i v_j \vartheta_{ij}^k + {v_j}^2 \vartheta_j^0 + 2\sigma_{vel}^2 \end{aligned} \tag{45}$$

where we used the properties of the Gamma function and the scaling factor

$$N_k = \int_{x_i=0}^{\infty} \int_{x_j=0}^{\infty} D_i^2(x_i) D_j^2(x_j) f_i(x_i) f_j(x_j) x_i^k \mathrm{d}x_i \mathrm{d}x_j \tag{46}$$

Integrating equations (38) to (40) and again using the properties of the Gamma function we finally obtain an analytical solution for the collision rate

$$\begin{aligned} &\left.\frac{\partial n_s}{\partial t}\right|_{coll,ij} = -\left.\frac{\partial n_i}{\partial t}\right|_{coll,ij} = -\left.\frac{\partial n_j}{\partial t}\right|_{coll,ij} \\ &= \frac{\pi}{4} E_{coll} n_i n_j \left[{D_i}^2 \delta_i^0 + D_i D_j \delta_{ji}^0 + {D_j}^2 \delta_j^0\right] / v_{ij,0} \end{aligned} \tag{47}$$

and the change of mass mixing ratios due to aggregation

$$\left.\frac{\partial q_i}{\partial t}\right|_{coll,ij} = -\frac{\pi}{4} E_{coll} q_i n_j \left[{D_i}^2 \delta_i^1 + D_i D_j \delta_{ji}^1 + {D_j}^2 \delta_j^0\right] / v_{ij,1} \tag{48}$$

https://doi.org/10.5194/egusphere-2024-2157
Preprint. Discussion started: 2 September 2024

$$\left.\frac{\partial q_j}{\partial t}\right|_{coll,ij} = -\frac{\pi}{4} E_{coll} q_j n_i \left[{D_i}^2 \delta_i^0 + D_i D_j \delta_{ij}^1 + {D_j}^2 \delta_j^1\right] / v_{ji,1} \tag{49}$$

$$\left.\frac{\partial q_s}{\partial t}\right|_{coll,ij} = -\left.\frac{\partial q_i}{\partial t}\right|_{coll,ij} - \left.\frac{\partial q_j}{\partial t}\right|_{coll,ij} \tag{50}$$

See Appendix C for the notation of the coefficients.

https://doi.org/10.5194/egusphere-2024-2157
Preprint. Discussion started: 2 September 2024

3 Idealised simulations

Name	Experiment
HA	HA15 het. ice nucleation
UL	UL18 het. ice nucleation
PH	PH08 het. ice nucleation
PH3	PH08 het. ice nucleation with soot and bio mode
REF	reference simulation with original SB scheme

Table 1. List of sensitivity experiments for idealised simulations

Idealised simulations of a deep convective cloud were conducted with the ICON model (Heinze et al., 2017). The Weisman-Klemp setup (Weisman and Klemp, 1982) (WK82) is a suitable test environment to evaluate the ice mode scheme microphysics as all particle classes and associated model routines are active in the simulation and both mixed-phase and pure ice clouds, the latter mostly located in the anvil, are observed.

The vertical profiles of temperature and relative humidity are chosen following Weisman and Klemp (1982) to represent a typical sounding of a deep convection event with a maximum water vapor mixing ratio near the surface of $0.014\,\mathrm{kg kg}^{-1}$ and a surface temperature of $300\,\mathrm{K}$. The horizontal wind u_z varies with altitude from 0 to $U_s = 5\,\mathrm{ms}^{-1}$ Convection was initiated with a symmetric thermal perturbation of $1400\,\mathrm{m}$ vertical extent and $10\,000\,\mathrm{m}$ diameter with an temperature amplitude of $2\,\mathrm{K}$ at the center, that decays to $0\,\mathrm{K}$ at the edge of the bubble.

The effective horizontal resolution of the unstructured triangular grid is $1.23\,\mathrm{km}$ with 128 vertical levels and a time step of $2\,\mathrm{s}$. The simulation time for each experiment is $240\,\mathrm{min}$.

Experiments with the ice modes scheme in several configurations were performed to evaluate the impact of different heterogeneous nucleation schemes on the distribution of the ice modes and the liquid origin vs in-situ formation pathway. Table 1 lists all experiments. HA, UL and PH label experiments using the nucleation schemes of Hande et al. (2015), Ullrich et al. (2017) and Phillips et al. (2008), respectively. The choice of parameters for the dust aerosol profiles are explained in Section 2.2.4. PH3 refers to a simulation with the Phillips et al. (2008) parametrisation including the soot and biological aerosol modes. The reference simulation (REF) uses the standard SB scheme with the same microphysical parametrisations and assumptions employed as the ice mode microphysics scheme. Thus we can assess the ramifications of using multiple ice classes instead of a single one for the overall cloud evolution.

3.1 Ice modes simulation

Figure 3 show the temporal evolution of the different hydrometeor classes as the average (Ice) Water Path (I)WP (a,b) and vertically integrated number densities (I)WPN (c,d) beneath the cloud system. Ice is displayed as the sum of all ice modes. Note that the output interval of the model is $10\,\mathrm{min}$ and we only display average Water Path values above $10^{-6}\,\mathrm{kg\,m}^{-2}$. Hence the plots only show the time where hydrometeor classes appear in an 'significant' amount.

https://doi.org/10.5194/egusphere-2024-2157
Preprint. Discussion started: 2 September 2024

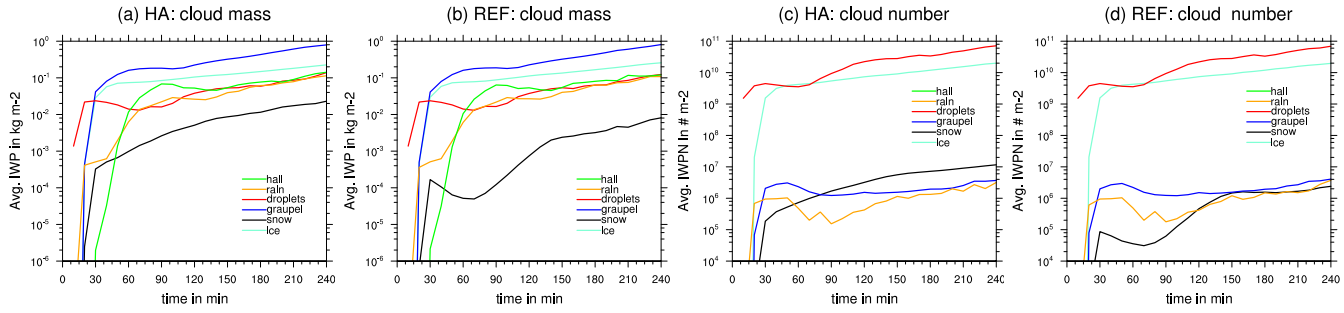

Figure 3. Temporal evolution of the average ice water path for each hydrometeor class for (a) ice modes (HA) and (b) reference SB simulation (REF). Temporal evolution of average integrated number density for (c) HA and (d) REF. ICE is the sum of all ice modes for HA.

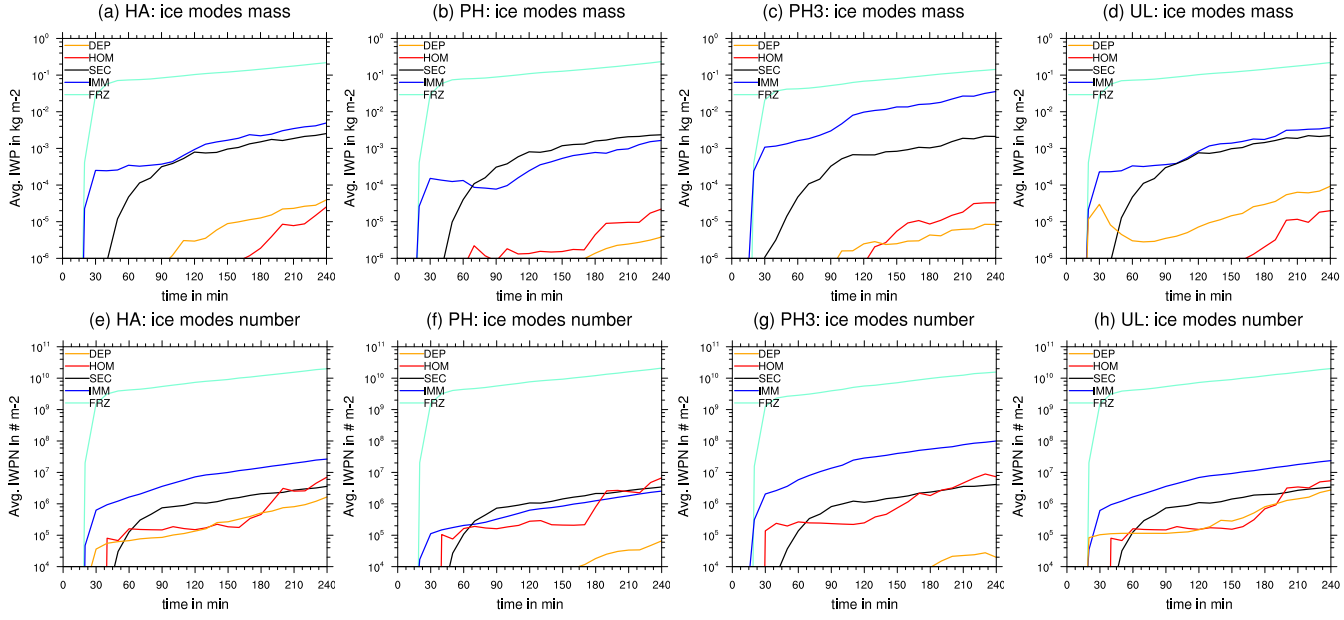

Figure 4. Temporal evolution of the average (ice) water path for each ice for heterogeneous ice nucleation scheme (a) HA, (b) PH, (c) PH3 and (d) UL. Average integrated number density for each ice mode for e) HA, (f) PH, (g) PH3 and (h) UL.

First we look at the evolution of the ice modes simulation (HA) in Panel (a). Cloud droplets condense within the first 10 min of the simulation followed by the initiation of the warm rain process. Ice and graupel appear at the same time around 18 min and become quickly the two major contributors to the Water Path. Aggregation occurs shortly after. Strong riming is the last microphysical process to become active with hail first occurring at 30 min. At 60 min simulation time the cell matures. The
475 average water path of each class remains slightly increasing and the cell shows no signs of dissipation within the simulation time. The ratio of the average water path between the classes also remain mostly the same with graupel followed by cloud ice being the dominate classes and hail, rain and cloud droplets showing mostly the same average values. Snow is the weakest

https://doi.org/10.5194/egusphere-2024-2157
Preprint. Discussion started: 2 September 2024

hydrometeor class. The mass density of cloud particles is primarily governed by the availability of supersaturation and thus thermodynamics. The number density on the other hand is more varied since it directly depends on the particle formation pathway. Panel (c) in Figure 3 shows the average integrated number densities of all hydrometeor classes. We observe a large gap between droplets and ice to the other classes. Droplet numbers are tied to the CCN (cloud condensation nuclei) activation scheme of Hande et al. (2016), which depends mainly on upward vertical velocity and thus produces a large number of droplets in a strong convective case like the Weisman-Klemp setup. However, the scheme is still limited by the number of available CCN. We will discuss the connection between high ice and droplet number densities below.

Figure 4 (a) provides insight into the development of each ice mode as average IWP and IWPN. At the beginning, ice consists of frozen cloud droplets where both immersion and homogeneous freezing, represented by the IMM and FRZ mode, respectively, are important. The latter, however, becomes the most dominant ice mode by several orders of magnitude. Secondary ice from rime splintering (SEC) occurs with a $20\,\mathrm{min}$ offset to the first occurrence of graupel and becomes almost as important as immersion freezing. This is consistent with the findings of Miltenberger et al. (2020), who also performed simulations with the ice mode schemes for the same test case, but utilized lagrangian trajectory analysis to investigate rime splintering and spread of secondary ice through the cloud system. The first occurrence of secondary ice of significant number concentrations ($n_{sec} > 0.1\,\mathrm{L}^{-1}$) was observed after $30\,\mathrm{min}$ even for simulations of higher wind shear. They found that riming with graupel that sedimented from higher levels into the Hallett-Mossop temperature zone ($265 < T < 270\,\mathrm{K}$) to be the dominant source of secondary ice.

Ice from homogeneous (HOM) and deposition nucleation (DEP) occurs first from nucleation events in the overshoot starting at $30\,\mathrm{min}$ and $40\,\mathrm{min}$ for DEP and HOM, respectively. Both types of nucleation events occur multiple times during the simulation and the average IWP of both modes increases over time. The DEP mode is overall stronger in terms of average IWP although the HOM mode catches up. It is also to note while the average IWP of HOM and DEP is weak, their average IWPN is much closer to the other modes, especially secondary ice, as can be seen in Figure 4 Panel (e). In general all ice modes except for FRZ show more similar values (in terms of orders of magnitude) when comparing average IWPN than when comparing average IWP. The IWPN of FRZ dominates and thus the total ice number density is strongly tied to the high number of droplets that the CCN activation scheme produces.

To investigate the vertical distribution of cloud particles Figure 5 shows a vertical slice of the cloud after $200\,\mathrm{min}$ simulation time and the mass densities of all hydrometeor classes, where ice is represented as the sum of all ice modes. The red and blue contours show the critical LWC and IWC value of $0.1\,\mathrm{mg\,m}^{-3}$, respectively. The developed convective cell has an vertical extent of $15\,\mathrm{km}$ and developed an anvil. The storm produces heavy (rain) precipitation beneath the cell. Most of the cloud is glaciated with rimed particles, mainly graupel, being the most prevalent in terms of mass. Hail is mostly found in the narrow updraft core where riming rates and resident times are highest. Ice is present in most parts of the cloud above the melting temperature and forms an anvil of (pure) ice with an overshooting top. The mass content of snow depends on the mass density and number concentrations of ice. However, it is heavier than snow and has higher sedimentation rates. Thus snow is mostly located below the maximum ice mass density.

https://doi.org/10.5194/egusphere-2024-2157
Preprint. Discussion started: 2 September 2024

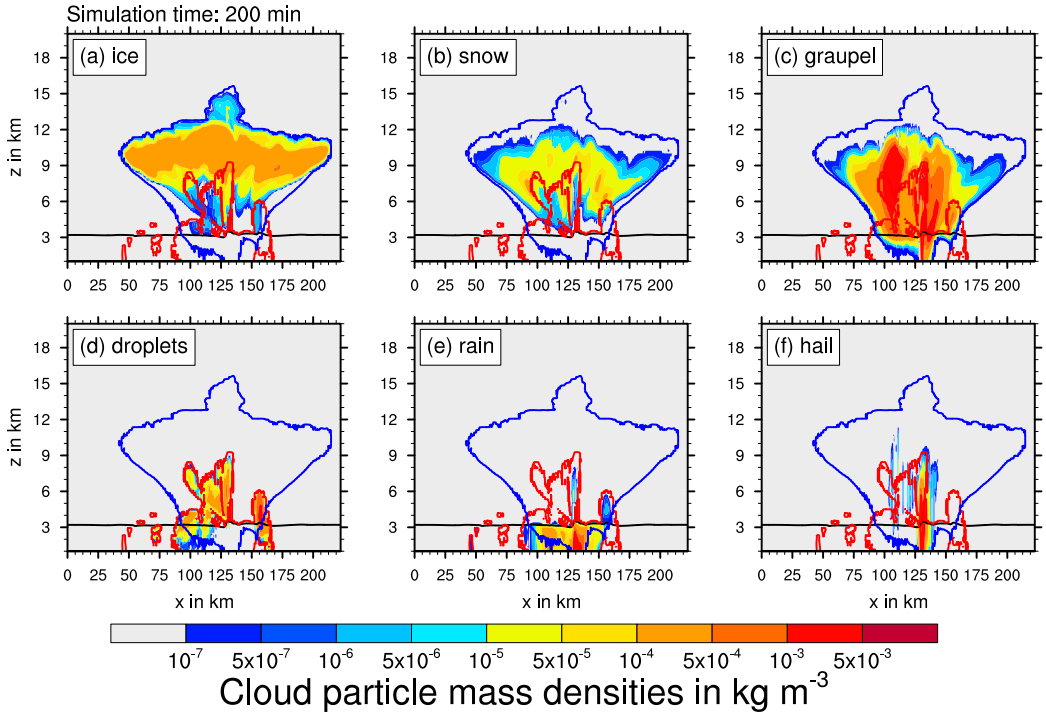

Figure 5. Weisman-Klemp test at 200 min simulation time. Mass densities of (a) total ice, (b) snow, (c) graupel, (d) cloud droplets, (e) raindrops and (f) hail. The black line indicates the melting temperature level. The red and blue contour show the critical LWC and IWC value of $0.1\,\mathrm{mg\,m^{-3}}$, respectively.

Figure 6 shows the same vertical slice as in Figure 5 but for the mass mixing ratio for each ice mode after 200 min simulation time. The lower part of the cloud is dominated by secondary ice from rime splintering (SEC) which coincides with the high mass mixing ratios of graupel and hail that we observed in Figure 5. The prevalence of secondary ice from rime splintering in this region was also observed by Miltenberger et al. (2020).

Ice in an altitude between 6 and 9 km is partially dominated by heterogeneously frozen droplets (IMM), while in the upper part of the cloud homogeneously frozen droplets (FRZ) are prevalent. When cloud droplets are transported upwards into colder regions they freeze first through immersion freezing due to the lower temperature threshold. Once all the INPs are activated, there is still a significant number of cloud droplets left or provided by the constant supply of humidity from convection. At this point homogeneous freezing begins to dominate over immersion freezing. Also, the ice mode schemes only shows the ice formation pathway of the ice observed at this time, it does not track sources and sinks individually. That means that ice from immersion freezing (IMM) could have been converted to snow by aggregation or lost in collisions with graupel and is for that reason not as prevalent as FRZ.

The part of the cloud consisting of ice from FRZ stays structurally mostly the same during the simulation run time, only

https://doi.org/10.5194/egusphere-2024-2157
Preprint. Discussion started: 2 September 2024

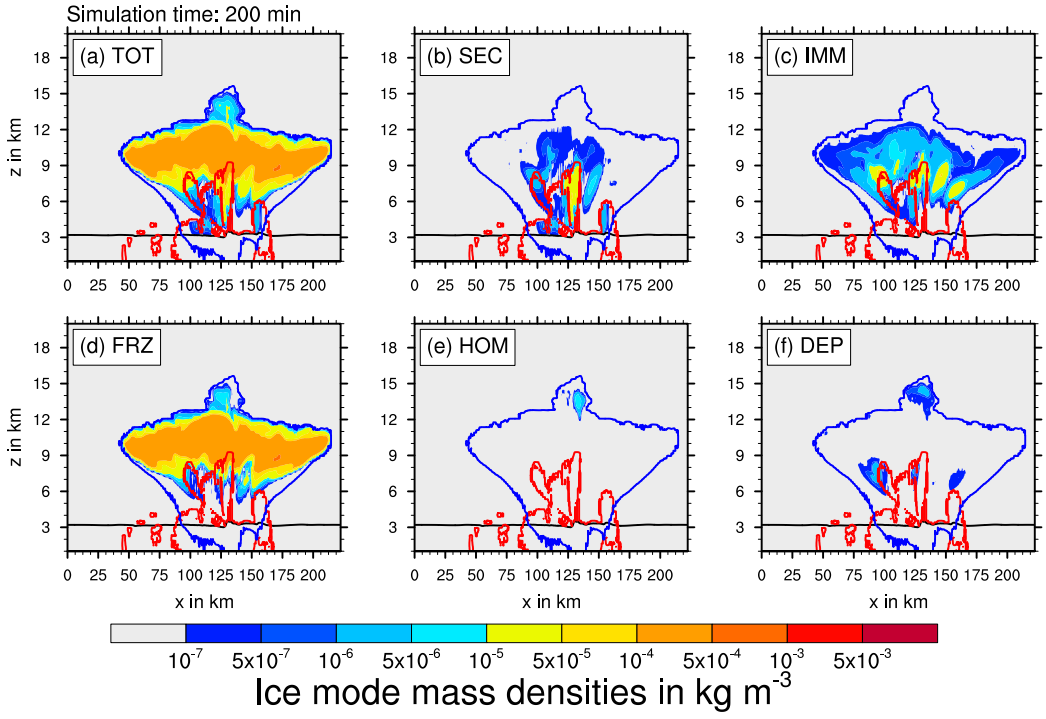

Figure 6. Weisman-Klemp test at 200 min simulation time. Mass densities of (a) sum of all ice modes, (b) secondary ice, (c) heterogeneously frozen droplets, (d) homogeneously frozen droplets, (e) homogeneous nucleation and (f) deposition nucleation. The black line indicates the melting temperature level. The red and blue contours show the critical LWC and IWC value of $0.1\,\mathrm{mg\,m^3}$, respectively.

widening as the anvil expands. However, the cloud parts where IMM and SEC are present fluctuate with the evolution of the cell. SEC follows the liquid core where riming is occurring. IMM is at the beginning located above the liquid core between the sections were SEC and FRZ are prevalent and later mostly present in the flanks.

Ice from homogeneous nucleation (HOM) is limited to the overshoot, deposition nucleation (DEP) also occurs in small amounts outside the liquid core in the glaciated parts of the cloud between 6 and 9 km.

Overall we notice a mostly clear spatial separation of the ice modes with some overlapping areas where ice of different origin is found. Ice in the upper part of the cloud above 9 km is for the majority of liquid origin, hence consisting of frozen droplets, and stemming from rime splintering below that. This general spatial distribution of the ice modes is also true for the other sensitivity experiments.

https://doi.org/10.5194/egusphere-2024-2157
Preprint. Discussion started: 2 September 2024

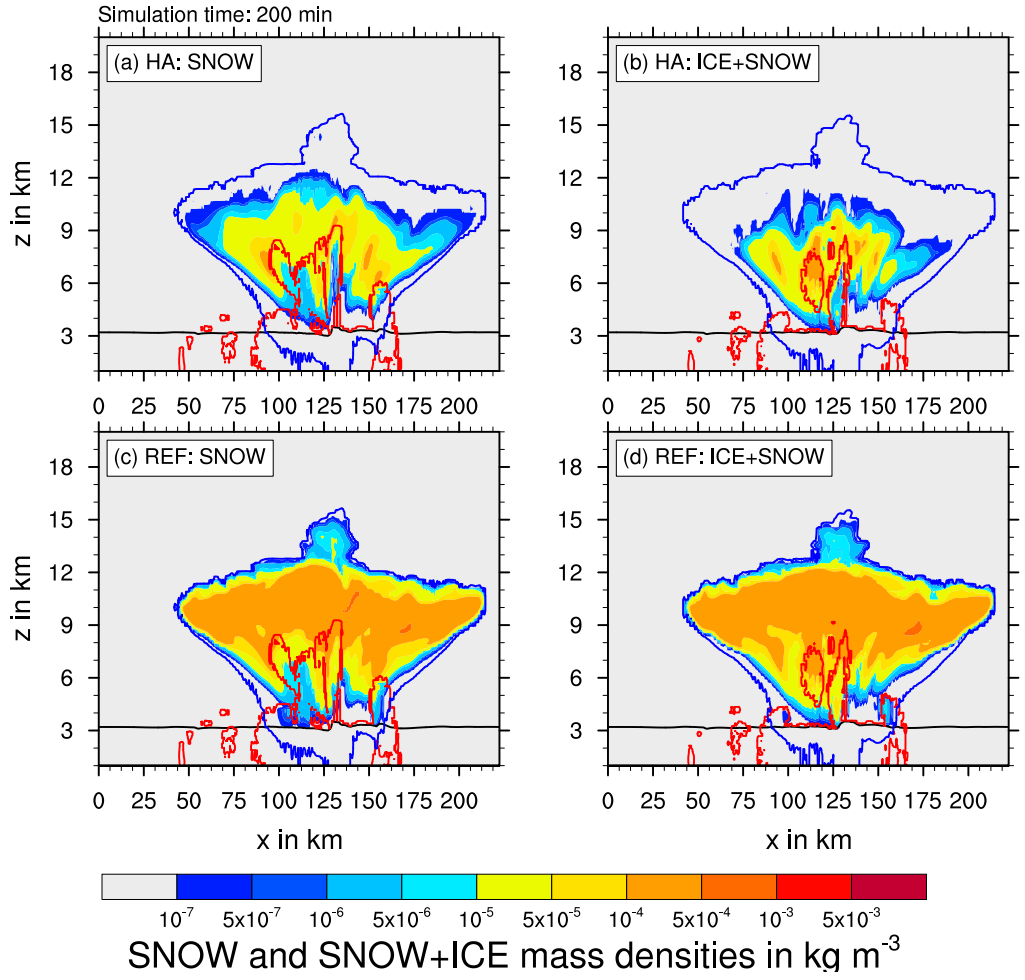

Figure 7. Weisman-Klemp test at 200 min simulation time. Mass densities of snow for (a) ice modes scheme (HA) and (c) standard SB (REF) as well as the sum of all cloud ice and snow for (b) HA and (d) REF. The black line indicates the melting temperature level. The red and blue contour show the critical LWC and IWC value of $0.1\,\mathrm{mg\,m^{-3}}$, respectively.

3.2 Comparison - reference simulation

The overall cloud evolution of the reference simulation (REF) is very close to the ice modes scheme. As we can see in Figure 3 (b) the evolution of hydrometeors directly related to the liquid phase, that is cloud droplets, rain, graupel and hail, show the same temporal evolution. Even the onset times for cloude ice, where the governing parametrisations of both schemes differ, are are mostly the same. We observe, however, a large difference in the average Water Path of snow which shows an increase of an order of magnitude for the simulation with the ice modes scheme (HA). Although the difference decreases with time to a factor of ~ 2.5.

https://doi.org/10.5194/egusphere-2024-2157
Preprint. Discussion started: 2 September 2024

This also evident in the vertical slice of the convective cloud. Figure 7 shows the vertical slice of the convective cloud at $200\,\mathrm{min}$ for snow with (a) the ice modes simulation and (c) the reference simulation. There is significantly more snow present in the ice mode simulation than in the reference simulation. While the maximum snow mass density is still at $10^4\,\mathrm{kgm}^3$, snow is distributed over a wider area of the cloud especially towards the flanks. But comparing the sum of ice and snow for both simulations in panels (b) and (d) shows that there is in general no increase of combined ice particle mass. Rather we notice there is a tendency for the ice mode scheme to shift mass from the ice to the snow class, hence the aggregations rate have to be higher. This is linked to the conceptional differences between both schemes: the SB standard scheme only produces snow by self collection of a single cloud ice class, where in the ice mode schemes, there are five independent cloud ice classes. They not only aggregate snow by self collection, but also by collisions with each other. While the physics of self collection and ice mode - ice mode collision are the same, the increased number of collisions processes leads to higher aggregation rates.

While the shift of ice to snow should affect overall sedimentation rates of ice particles, there seems to be little impact on the cloud evolution and dynamics of the convective cell since the IWC and LWC outlines as well as the general evolution of the cloud observed in Figure 3 remains the same. It is also to note that pure ice and especially cirrus clouds will be mostly unaffected by that effect since collision efficiencies are small at low temperatures (see Section 2.5.2). Generally ice number concentrations are also insufficient to produce significant amounts of snow for pure ice clouds. Indeed, we will observe in later sections that snow is mostly insignificant in simulations of cirrus clouds even with the 'bias' of the ice modes scheme. Still we should keep this tendency towards higher snow content in mind when simulating deep convection clouds and consider to scale aggregation rates accordingly.

https://doi.org/10.5194/egusphere-2024-2157
Preprint. Discussion started: 2 September 2024

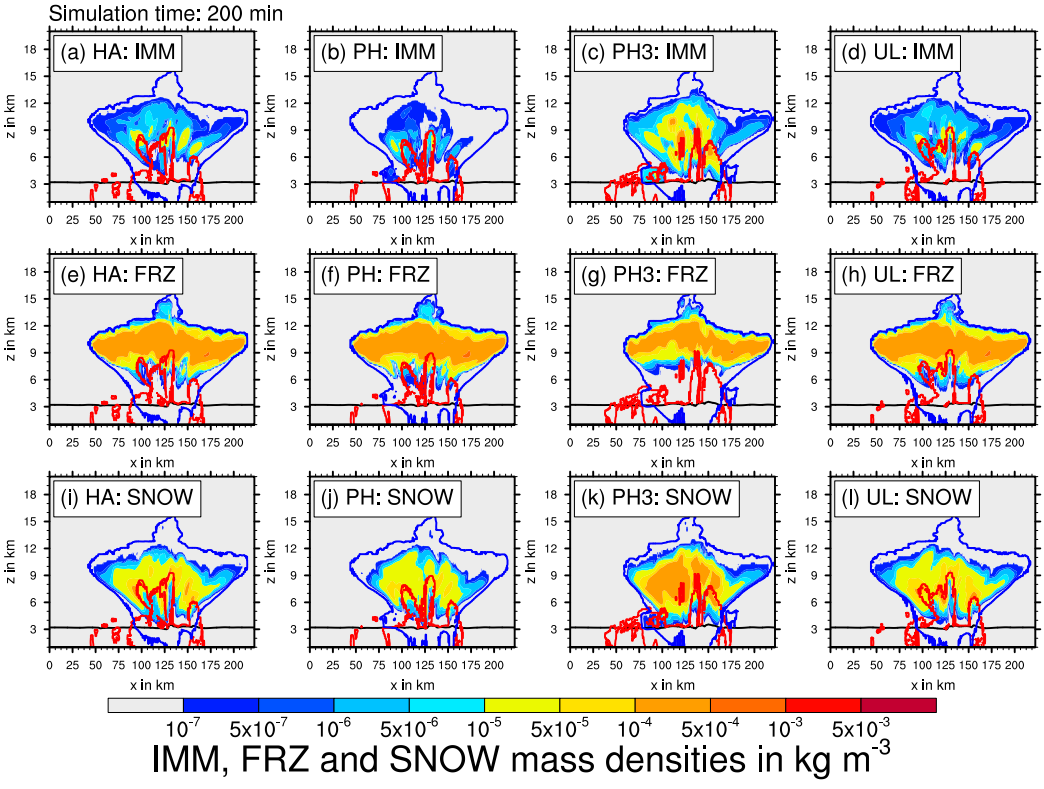

Figure 8. Weisman-Klemp test at 200 min simulation time comparing mass densities of IMM (a-d), FRZ (f-h) and snow (i-l) for the experiments HA (a,e,i), PH (b,f,j), PH3 (c,g,k) and UL (d,h,l). The black line indicates the melting temperature level. The red and blue contour show the critical LWC and IWC value of $0.1\,\mathrm{mg\,m^{-3}}$, respectively.

https://doi.org/10.5194/egusphere-2024-2157
Preprint. Discussion started: 2 September 2024

3.3 Comparison - heterogeneous ice nucleation

Change of assumptions regarding distribution of INPs or a switch to a different INP activation scheme entirely can have a large impact on the evolution of the ice phase. We compared HA, PH, PH3 and UL. For the general evolution of average Cloud Water Path and Ice Water Path, we do not observe major differences. Hence we will discuss the general evolution of the convective cloud only briefly here. Since the same CCN activation is used for all runs we do not observe much change for the evolution of the liquid phase. The Rain Water Path is slightly lower for PH after the initial warm-rain formation, but catches up later. Hail formation starts sooner for PH but also reaches the same average value as HA. Further we observe a shift towards more snow and slightly less (total) ice for the PH simulation where in general all particle classes are much closer in terms of average Water Path. Thus the overall evolution of the convective clouds are similar.

We will now investigate the spatial and temporal distribution of the ice modes more closely. If we study the evolution of the ice modes average IWP in Figure 4 panels (a) to (d) we observe that FRZ and SEC stay mostly the same for all runs. SEC stems from rime splintering and thus depends on the evolution of the graupel and hail class, which again is sensitive to CCN activation and the resulting number of super-cooled droplets. We observed in Section 3.1 that SEC occupies a distinct part of the lower cloud around the updraft core. A change in heterogeneous nucleation scheme seems not to significantly affect the dominance of ice from rime splintering in this region or change the avg. IWP from secondary ice.

FRZ is strongly sensitive to the CCN activation scheme which remains unchanged between the simulations. A weaker IMM mode should affect FRZ since droplets that do not freeze by interacting with INP freeze homogeneously instead unless they are removed by evaporation or collision. Hence both modes are in direct competition for unfrozen cloud droplets. However, FRZ is overall so dominant in this case study, that this effect is not noticeable with regards to averaged mass content and number concentrations.

IMM is weaker in the simulation with the PH scheme both for average IWP and IWPN (Panel b and f), while it stays the same for HA and UL. The latter is not surprising since the assumptions about immersion freezing and the number concentrations of INPs are almost the same. In Section 2.2.4 we chose the dust concentration parameters for the PH parametrisation such that the maximum number of INPs activated for immersion freezing were the same as for the UL and HA schemes. The important difference of the PH to the HA and UL schemes is that immersion freezing occurs at higher temperatures (close to 263 instead of $258\,\mathrm{K}$). Thus in lower and warmer parts of the cloud, where hydrometeor classes other than cloud ice are abundant, e.g. graupel. Collisions with those classes are an efficient sink for the IMM mode. Hence the average IWP and IWPN of IMM are smaller for PH compared to HA and UL.

For PH3 (Panel c and h) we observe higher average IWP of IMM than for all other simulations. Even though we stated in Section 2.2.4 that the maximum amount of active INP is lower with this scheme then for the others, the inclusion of soot and biological aerosols triggers immersion freezing at higher temperatures even close to the melting temperature level $T_m = 273\,\mathrm{K}$. Where for the PH scheme with the dust only mode, the shift to higher activation temperatures lowered the IMM content, for PH3, with the soot and biological aerosol mode, IMM content is increased. Likely this even 'earlier' activation of INPs changes the cloud evolution such that the IMM mode becomes more important. Indeed, we will note that the cloud shape is different

https://doi.org/10.5194/egusphere-2024-2157
Preprint. Discussion started: 2 September 2024

for PH3 when we later present a vertical slice of the cloud.

DEP is in generally weak in this convective case since deposition nucleation events only trigger outside mixed-phase clouds (see Section 2.2.4). In Figure 4 we observe different triggering times and strengths of deposition nucleation events. However, these differences are mostly caused by non-linear realisations of the model dynamics and not sensitive to the choice of nucleation scheme.

While DEP is not continuously persistent in the overshoot, there are smaller nucleation events being triggered in the anvil and the flanks of the convective cloud. Also note that output is written only every $10\,\mathrm{min}$, hence not all nucleation events are sampled in the output data and ice from DEP and HOM could be removed by aggregation before they are sampled. When using the PH or PH3 scheme DEP is almost not present at all. This is consistent with our description of the scheme in Section 3.1, where even weak nucleation events are only triggered at high S_i compared to UL and HA. Consequently, the HOM mode is strengthened for PH since homogeneous nucleation events are not suppressed by pre-existing ice from DEP.

Figure 8 shows vertical slices of the cloud at $200\,\mathrm{min}$. Plotted are the mass content of ice from immersion freezing (IMM) and homogeneously frozen droplets (FRZ) as well as snow for HA, PH, PH3 and UL (first, second, third and fourth column, respectively). As already discussed, FRZ dominates the upper part of the convective cloud for all heterogeneous nucleation schemes. The structure of vertically layered ice modes described in Section 3.1 holds true for all simulations. As immersion freezing is mostly the same for HA and UL the distribution of ice modes and snow shows only marginal differences between both experiments (first and fourth column).

For PH, however, we found that IMM is much weaker in terms of mass content (and number densities). That also limits its horizontal distribution, which is confined more towards the core of the cloud compared to HA and UL. This directly affects the snow class, which shows lower number densities and less spreading throughout the cloud. This underlines again, that IMM is important for aggregation because it produces ice crystals large enough for efficient collection kernels (see Section 2.5.2).

Using PH3 affects not only the IMM mode but also the overall structure of the cloud. As discussed above, PH3 favors immersion freezing and its biological and soot INP modes show an onset for higher temperatures compared to other heterogeneous ice schemes. We observe the result of INP activation at higher temperatures with a shift of ice mass towards the lower model levels. This can also be observed in the shape of the convective cloud. For example the PH3 cloud shows a lesser developed left flank. Additionally there is a pocket of IMM ice above the melting temperature line which is not present for HA and UL, for which immersion freezing is not possible in this temperature region. While the general structure and layering of ice modes is the same, the shape and location of liquid water zones change (as can be seen from the red LWC outlines) which has a direct effect on the SEC mode that in general follows the liquid core (where riming occurs) closely. The PH3 simulation also sees an increase in snow underlining the importance of aggregation as a sink for the (in PH3 stronger) IMM mode.

https://doi.org/10.5194/egusphere-2024-2157
Preprint. Discussion started: 2 September 2024

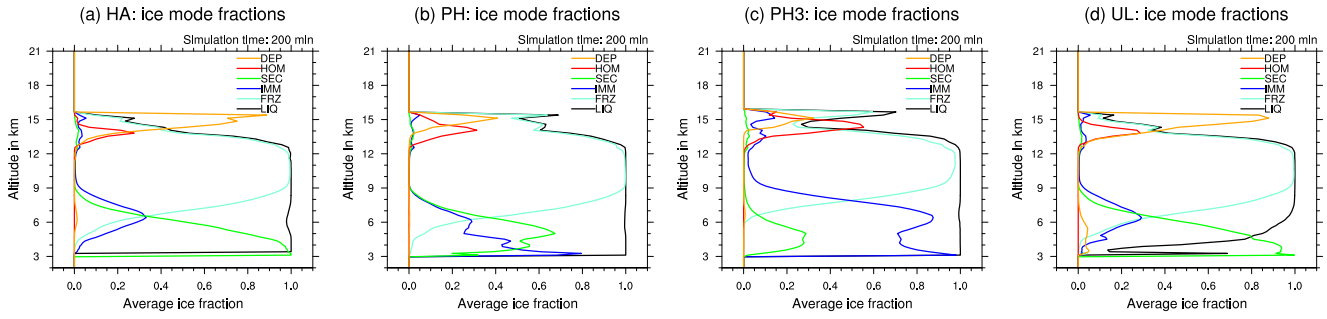

Figure 9. Average liquid origin and ice mode fractions for (a) HA, (b) PH, (c) PH3, (d) UL.

3.4 Liquid origin vs in-situ formation

Figure 9 shows the average mass fraction for all ice modes at $200\,\mathrm{min}$ simulations time. The mass fraction describes the ratio of ice from a particular mode x to the total cloud ice q_{tot} (sum of all ice modes)

$$f_x = \frac{q_x}{q_{tot}} \tag{51}$$

LIQ is the liquid origin fraction describing the ratio of cloud ice stemming from liquid origin formation processes

$$f_{liq} = \frac{q_{frz} + q_{imm}}{q_{frz} + q_{imm} + q_{hom} + q_{dep}} \tag{52}$$

where HOM and DEP contribute to in-situ formed cirrus and the FRZ and IMM to liquid origin cirrus. Secondary ice is excluded here.

The majority of the fully glaciated parts of the cloud above the secondary ice region between 6 and $12\,\mathrm{km}$ is dominated by IMM (for HA, PH and UL) or FRZ (for PH3) classifying the parts of (pure) ice cloud as liquid origin (hence LIQ is close to 1). This includes the anvil of the deep convective cloud. The overshoot is located above $12\,\mathrm{km}$ and the liquid origin fraction is determined by the amount of FRZ ice being mixed into this region and the strength of DEP nucleation events. PH and PH3 show a weak DEP mode with incursions from HOM resulting in liquid origin fractions between 0.3 and 0.7. For HA and UL the liquid origin fraction is below 0.4. This makes the overshoot a region where ice stemming from different formation pathways mixes. The dynamic forcing transporting FRZ and IMM ice into the overshoot, the occurrence and strength of HOM and DEP nucleation events and the sedimentation of newly formed ice from the overshoot into the cloud below all affect and change the liquid origin fraction. That the majority of the fully glaciated parts of the deep convection cloud are of liquid origin is in accordance with previous studies (Gasparini et al., 2018).

https://doi.org/10.5194/egusphere-2024-2157
Preprint. Discussion started: 2 September 2024

4 Discussion and Summary

We presented a new microphysics bulk model adapted from the SB two-moment scheme by introducing multiple ice classes each with their unique particle formation mechanism: homogeneous freezing of solution and pure water droplets, immersion freezing, deposition nucleation and secondary ice from rime splintering. The microphysical processes governing these ice modes have been described with an emphasis on the particle formation mechanisms.

Idealised simulations of an convective cloud, using the Weisman-Klemp setup, were performed to validate the model with an comparison to a reference simulation using the standard SB scheme. It was shown that the ice mode schemes reproduces the same cloud evolution for the dynamics and all particle classes except for snow, where we observed a shift of mass content from ice crystals to snow. This is linked to an increase of collision processes due to introduction of multiple ice classes.

We found that the scheme showed a reasonable distribution of the ice modes with liquid origin ice, formed of homogeneously and immersion frozen droplets, to constitute the majority of ice present in the matured cell. The occurrence of in-situ ice formed of homogeneous and deposition nucleation origin was, compared to other modes, low as it is expected for a convective cloud. Most in-situ ice modes were only present in the overshoot. But even there they mixed with liquid origin ice modes that were transported into the overshoot.

Simulations with four different heterogeneous nucleation parametrisations showed that the ice mode scheme provides the basis for a nuanced analysis to evaluate the impact of parametrisation choice not only on the total ice content and number concentrations but on the competition between ice particle formation pathways as well.

We investigated rime splintering as a secondary ice mechanism. In general we observed that it not significantly enhanced ice content in parts of the convective clouds were primary ice formation is active. Rather secondary ice was relevant in thermodynamic regions where primary ice formation is insufficient. Thus it helped to expand cloud ice especially towards higher temperature levels. However, we note that the importance and high number densities of secondary ice from RS in the lower parts of the cloud (below 7 km) are concerning since the underlying parametrisation of Hallett-Mossop could not be confirmed by recent laboratory studies (Seidel et al., 2024).

In a future work we will implement additional secondary ice processes, droplet shattering and collisional breakup, and investigate their relevance in idealised as well as synoptic-scale simulations. We further want to study origin of cloud ice in the cloud band and outflow region of Warm Conveyor Belts especially addressing the open research question of in-situ vs liquid origin cirrus.

Code availability. The NCL code for the data evaluation is available upon request.

Data availability. All data are available from the authors upon request.

https://doi.org/10.5194/egusphere-2024-2157
Preprint. Discussion started: 2 September 2024

Appendix A: List of abbreviations

Abbreviation	Description
DEP	deposition nucleation ice mode
FRZ	homogeneous freezing of cloud droplets ice mode
HA15	Hande et al. (2015) ice nucleation scheme
HOM	homogeneous freezing of solution droplets ice mode
IMM	immersion freezing ice mode
IWC	ice water content
IWP	ice water path
IWPN	vertically integrated ice number density
LWC	liquid water content
PH08	Phillips et al. (2008) ice nucleation scheme
UL17	Ullrich et al. (2017) ice nucleation scheme
SB	Seifert and Beheng (2006) double-moment scheme
SEC	secondary ice mode
TOT	sum of all ice modes

Table A1. List of abbreviations

Appendix B: Generalized Gamma distribution

The generalized gamma distribution is used to describe the mass or size distribution of a cloud particle class

$$f(x) = Ax^{\nu} \exp(-\lambda x^{\mu}) \tag{B1}$$

where we use the particle mass x as the variable and the shape and scale parameters ν and μ are prescribed. λ and A are linked to the prognostic distribution moments, the zeroth and first moment, corresponding to the number density $M^0 = n$ and mass mixing ratio $M^1 = q$, respectively. To obtain the n-th mass weighed moment of the generalized gamma distribution M^n we multiply equation (B1) with x^n and integrate over the entire domain which yields

$$\begin{aligned} M^n &= \int_0^{\infty} f(x) x^n \,\mathrm{d}x = \int_0^{\infty} Ax^{\nu+n} \exp(-\lambda x^{\mu}) \,\mathrm{d}x \\ &= \frac{A}{\mu} \int_0^{\infty} y^{\frac{\nu+n+1}{\mu}-1} \exp(-\lambda y) \,\mathrm{d}y \\ &= \frac{A}{\mu \lambda^{\frac{\nu+n+1}{\mu}}} \Gamma\left(\frac{\nu+n+1}{\mu}\right) \end{aligned} \tag{B2}$$

https://doi.org/10.5194/egusphere-2024-2157
Preprint. Discussion started: 2 September 2024

where we used the substitution $y = x^{\mu}$ and the relation of the Gamma function $\int_0^{\infty} y^{\zeta} \exp(-\eta y)\,\mathrm{d}y = \Gamma(\zeta+1)\eta^{-(\zeta+1)}$ for $\zeta > -1$, which can be reduced to Euler's definition of the Gamma function with the use of a suitable substitution.
Prescribing constant values for the shape parameters ν and μ we can now solve equation (B2) for A and λ

$$\lambda = \left(\frac{n}{q} \frac{\Gamma\left(\frac{\nu+2}{\mu}\right)}{\Gamma\left(\frac{\nu+1}{\mu}\right)} \right)^{\mu} \tag{B3}$$

$$A = \frac{\mu n}{\Gamma\left(\frac{\nu+1}{\mu}\right)} \lambda^{\frac{\nu+1}{\mu}} = \frac{\mu n}{\Gamma\left(\frac{\nu+1}{\mu}\right)} \left(\frac{n}{q} \frac{\Gamma\left(\frac{\nu+2}{\mu}\right)}{\Gamma\left(\frac{\nu+1}{\mu}\right)} \right)^{\nu+1} \tag{B4}$$

and so we can finally describe the distribution function as a function of particle mass and the two prognostic moments

$$f(x,q,n) = \left[\frac{x}{x}\right]^{\nu} \frac{n}{\mu x \Gamma\left(\frac{\nu+1}{\mu}\right)} \left[\frac{\Gamma\left(\frac{\nu+2}{\mu}\right)}{\Gamma\left(\frac{\nu+1}{\mu}\right)} \right]^{\nu+1} \exp\left(- \left[\frac{x}{x} \frac{\Gamma\left(\frac{\nu+2}{\mu}\right)}{\Gamma\left(\frac{\nu+1}{\mu}\right)} \right]^{\mu} \right) \tag{B5}$$

with the mean particle mass $x = \frac{q}{n}$.

Appendix C: Notation collision integrals

These shorthand notations are used for the coefficients in the analytical results of the collision integrals in Section 2.5.2 and can be calculated beforehand since they only contain fixed parameters

$$\delta_i^k = \frac{\Gamma\left(\frac{2b_i+1+\nu_i+k}{\mu_i}\right)}{\Gamma\left(\frac{\nu_i+1}{\mu_i}\right)} \left(\frac{\Gamma\left(\frac{\nu_i+1}{\mu_i}\right)}{\Gamma\left(\frac{\nu_i+2}{\mu_i}\right)} \right)^{2b_i+k} \tag{C1}$$

$$\delta_{ji}^k = \frac{\Gamma\left(\frac{b_i+1+\nu_i+k}{\mu_i}\right)}{\Gamma\left(\frac{\nu_i+k}{\mu_i}\right)} \left(\frac{\Gamma\left(\frac{\nu_i+1}{\mu_i}\right)}{\Gamma\left(\frac{\nu_i+2}{\mu_i}\right)} \right)^{b_i+1} \frac{\Gamma\left(\frac{b_j+1+\nu_j}{\mu_j}\right)}{\Gamma\left(\frac{\nu_j+1}{\mu_j}\right)} \left(\frac{\Gamma\left(\frac{\nu_j+1}{\mu_j}\right)}{\Gamma\left(\frac{\nu_j+2}{\mu_j}\right)} \right)^{b_j} \tag{C2}$$

$$\vartheta_i^k = \frac{\Gamma\left(\frac{\nu_i+2b_i+1+2\beta_i+k}{\mu_i}\right)}{\Gamma\left(\frac{2b_1+1+\nu_i+k}{\mu_i}\right)} \left(\frac{\Gamma\left(\frac{\nu_i+1}{\mu_i}\right)}{\Gamma\left(\frac{\nu_i+2}{\mu_i}\right)} \right)^{2\beta_i} \tag{C3}$$

$$\vartheta_{ji}^k = \frac{\Gamma\left(\frac{\nu_j+2b_j+\beta_j+1}{\mu_j}\right)}{\Gamma\left(\frac{2b_j+1+\nu_j}{\mu_j}\right)} \left(\frac{\Gamma\left(\frac{\nu_j+1}{\mu_j}\right)}{\Gamma\left(\frac{\nu_j+2}{\mu_j}\right)} \right)^{\beta_j} \frac{\Gamma\left(\frac{\nu_i+2b_i+1+\beta_i+k}{\mu_i}\right)}{\Gamma\left(\frac{2b_i+1+\nu_i+k}{\mu_i}\right)} \left(\frac{\Gamma\left(\frac{\nu_i+1}{\mu_i}\right)}{\Gamma\left(\frac{\nu_i+2}{\mu_i}\right)} \right)^{\beta_i} \tag{C4}$$

https://doi.org/10.5194/egusphere-2024-2157
Preprint. Discussion started: 2 September 2024

Author contributions. TL and AS did the model development; TL and PS designed the study; TL performed the simulations and carried out the data analyses; TL and PS contributed to interpreting the results and writing the paper.

Competing interests. The contact author has declared that none of the authors has any competing interests.

Disclaimer. Publisher's note: Copernicus Publications remains neutral with regard to jurisdictional claims in published maps and institutional affiliations.

Acknowledgements. The research leading to these results has been done within the subproject B7 of the Transregional Collaborative Research Center SFB/TRR 165 Waves to Weather funded by the German Research Foundation (DFG).

Parts of this research were conducted using the supercomputer MOGON 2 and/or advisory services offered by Johannes Gutenberg University Mainz (hpc.uni-mainz.de), which is a member of the AHRP (Alliance for High Performance Computing in Rhineland Palatinate, www.ahrp.info) and the Gauss Alliance e.V.

The authors gratefully acknowledge the computing time granted on the supercomputer MOGON 2 at Johannes Gutenberg University Mainz (hpc.uni-mainz.de).

https://doi.org/10.5194/egusphere-2024-2157
Preprint. Discussion started: 2 September 2024

References

Barklie, R. H. D. and Gokhale, N. R.: The freezing of supercooled water drops, Stormy Weather Group, McGill Univ., Sci. Rep., MW-30, 43–64, 1959.

Bigg, E.: The formation of atmospheric ice crystals by the freezing of droplets, Quarterly Journal of the Royal Meteorological Society, 79, 510–519, https://doi.org/10.1002/qj.49707934207, 1953.

Choularton, T., Latham, J., and Mason, B. J.: A possible mechanism of ice splinter production during riming, Nature, 274, 791–792, https://doi.org/10.1038/274791a0, 1978.

Cotton, R. and Field, P.: Ice nucleation characteristics of an isolated wave cloud, Quarterly Journal of the Royal Meteorological Society: A journal of the atmospheric sciences, applied meteorology and physical oceanography, 128, 2417–2437, https://doi.org/10.1256/qj.01.150, 2002.

Cotton, W. R., Tripoli, G. J., Rauber, R. M., and Mulvihill, E. A.: Numerical Simulation of the Effects of Varying Ice Crystal Nucleation Rates and Aggregation Processes on Orographic Snowfall, Journal of Climate and Applied Meteorology, 25, 1658–1680, https://doi.org/10.1175/1520-0450(1986)025<1658:NSOTEO>2.0.CO;2, 1986.

Emersic, C. and Connolly, P.: Microscopic observations of riming on an ice surface using high speed video, Atmospheric Research, 185, 65–72, 2017.

Gasparini, B., Meyer, A., Neubauer, D., Münch, S., and Lohmann, U.: Cirrus Cloud Properties as Seen by the CALIPSO Satellite and ECHAM-HAM Global Climate Model, Journal of Climate, 31, 1983 – 2003, https://doi.org/10.1175/JCLI-D-16-0608.1, 2018.

Hallett, J. and Mossop, S. C.: Production of secondary ice particles during the riming process, Nature, 249, 26–28, https://doi.org/10.1038/249026a0, 1974.

Hande, L. B., Engler, C., Hoose, C., and Tegen, I.: Seasonal variability of Saharan desert dust and ice nucleating particles over Europe, Atmospheric Chemistry and Physics, 15, 4389–4397, https://doi.org/10.5194/acp-15-4389-2015, 2015.

Hande, L. B., Engler, C., Hoose, C., and Tegen, I.: Parameterizing cloud condensation nuclei concentrations during HOPE, Atmospheric Chemistry and Physics, 16, 12 059–12 079, https://doi.org/10.5194/acp-16-12059-2016, 2016.

Heinze, R., Dipankar, A., Henken, C. C., Moseley, C., Sourdeval, O., Trömel, S., Xie, X., Adamidis, P., Ament, F., Baars, H., et al.: Large-eddy simulations over Germany using ICON: A comprehensive evaluation, Quarterly Journal of the Royal Meteorological Society, 143, 69–100, https://doi.org/10.1002/qj.2947, 2017.

Hoose, C. and Möhler, O.: Heterogeneous ice nucleation on atmospheric aerosols: a review of results from laboratory experiments, Atmospheric Chemistry and Physics, 12, 9817, https://doi.org/10.5194/acp-12-9817-2012, 2012.

Jeffery, C. and Austin, P.: Homogeneous nucleation of supercooled water: Results from a new equation of state, Journal of Geophysical Research: Atmospheres, 102, 25 269–25 279, https://doi.org/10.1029/97JD02243, 1997.

Kärcher, B. and Lohmann, U.: A parameterization of cirrus cloud formation: Homogeneous freezing of supercooled aerosols, Journal of Geophysical Research: Atmospheres, 107, AAC–4, https://doi.org/10.1029/2001JD000470, 2002.

Kärcher, B., Hendricks, J., and Lohmann, U.: Physically based parameterization of cirrus cloud formation for use in global atmospheric models, Journal of Geophysical Research: Atmospheres, 111, https://doi.org/10.1029/2005JD006219, 2006.

Khvorostyanov, V.: Mesoscale processes of cloud formation, cloud-radiation interaction, and their modelling with explicit cloud microphysics, Atmospheric Research, 39, 1–67, https://doi.org/10.1016/0169-8095(95)00012-G, 1995.

Kobayashi, T.: On the Variation of Ice Crystal Habit with Temperatur, Physics of Snow and Ice: proceedings, 1, 95–104, 1967.

https://doi.org/10.5194/egusphere-2024-2157
Preprint. Discussion started: 2 September 2024

Koop, T., Luo, B., Tsias, A., and Peter, T.: Water activity as the determinant for homogeneous ice nucleation in aqueous solutions, Nature, 406, 611–614, https://doi.org/10.1038/35020537, 2000.

Korolev, A. and Leisner, T.: Review of experimental studies of secondary ice production, Atmospheric Chemistry and Physics, 20, 11 767–11 797, https://doi.org/10.5194/acp-20-11767-2020, 2020.

Krämer, M., Rolf, C., Luebke, A., Afchine, A., Spelten, N., Costa, A., Meyer, J., Zöger, M., Smith, J., Herman, R. L., Buchholz, B., Ebert, V., Baumgardner, D., Borrmann, S., Klingebiel, M., and Avallone, L.: A microphysics guide to cirrus clouds – Part 1: Cirrus types, Atmospheric Chemistry and Physics, 16, 3463–3483, https://doi.org/10.5194/acp-16-3463-2016, 2016.

Köhler, C. G. and Seifert, A.: Identifying sensitivities for cirrus modelling using a two-moment two-mode bulk microphysics scheme, Tellus B: Chemical and Physical Meteorology, https://doi.org/10.3402/tellusb.v67.24494, 2015.

Libbrecht, K. G.: The physics of snow crystals, Reports on progress in physics, 68, 855, 2005.

Macklin, W.: The production of ice splinters during riming, Nubila, 3, 30–33, 1960.

Magono, C. and Lee, C. W.: Meteorological classification of natural snow crystals, Journal of the Faculty of Science, Hokkaido University. Series 7, Geophysics, 2, 321–335, 1966.

Miltenberger, A. K., Lüttmer, T., and Siewert, C.: Secondary Ice Formation in Idealised Deep Convection—Source of Primary Ice and Impact on Glaciation, Atmosphere, 11, 542, https://doi.org/10.3390/atmos11050542, 2020.

Morrison, H., Curry, J., and Khvorostyanov, V.: A new double-moment microphysics parameterization for application in cloud and climate models. Part I: Description, Journal of the atmospheric sciences, 62, 1665–1677, https://doi.org/10.1175/JAS3446.1, 2005.

Niemand, M., Möhler, O., Vogel, B., Vogel, H., Hoose, C., Connolly, P., Klein, H., Bingemer, H., DeMott, P., Skrotzki, J., and Leisner, T.: A Particle-Surface-Area-Based Parameterization of Immersion Freezing on Desert Dust Particles, Journal of the Atmospheric Sciences, 69, 3077–3092, https://doi.org/10.1175/JAS-D-11-0249.1, 2012.

Phillips, V. T., DeMott, P. J., and Andronache, C.: An empirical parameterization of heterogeneous ice nucleation for multiple chemical species of aerosol, Journal of the atmospheric sciences, 65, 2757–2783, https://doi.org/10.1175/2007JAS2546.1, 2008.

Pruppacher, H., Klett, J., Pruppacher, H., and Klett, J.: Microstructure of atmospheric clouds and precipitation, Microphysics of clouds and precipitation, pp. 10–73, 2010.

Pruppacher, H. R. and Klett, J. D.: Microphysics of clouds and precipitation, Taylor and Francis, 1998.

Ren, C. and MacKenzie, A.: Cirrus parametrization and the role of ice nuclei, Quarterly Journal of the Royal Meteorological Society: A journal of the atmospheric sciences, applied meteorology and physical oceanography, 131, 1585–1605, https://doi.org/10.1256/qj.04.126, 2005.

Seidel, J. S., Kiselev, A. A., Keinert, A., Stratmann, F., Leisner, T., and Hartmann, S.: Secondary ice production – no evidence of efficient rime-splintering mechanism, Atmospheric Chemistry and Physics, 24, 5247–5263, https://doi.org/10.5194/acp-24-5247-2024, 2024.

Seifert, A.: Parametrisierung wolkenmikrophysikalischer Prozesse und Simulation konvektiver Mischwolken, Ph.D. thesis, Institut für Meteorologie und Klimaforschung, Universität Karlsruhe/Forschungszentrum Karlsruhe, 2002.

Seifert, A. and Beheng, K. D.: A two-moment cloud microphysics parameterization for mixed-phase clouds. Part 1: Model description, Meteorology and atmospheric physics, 92, 45–66, https://doi.org/10.1007/s00703-005-0112-4, 2006.

Spichtinger, P., Marschalik, P., and Baumgartner, M.: Impact of formulations of the homogeneous nucleation rate on ice nucleation events in cirrus, Atmospheric Chemistry and Physics, 23, 2035–2060, https://doi.org/10.5194/acp-23-2035-2023, 2023.

Steinke, I., Hoose, C., Möhler, O., Connolly, P., and Leisner, T.: A new temperature- and humidity-dependent surface site density approach for deposition ice nucleation, Atmospheric Chemistry and Physics, 15, 3703–3717, https://doi.org/10.5194/acp-15-3703-2015, 2015.

https://doi.org/10.5194/egusphere-2024-2157
Preprint. Discussion started: 2 September 2024

Ullrich, R., Hoose, C., Möhler, O., Niemand, M., Wagner, R., Höhler, K., Hiranuma, N., Saathoff, H., and Leisner, T.: A New Ice Nucleation Active Site Parameterization for Desert Dust and Soot, Journal of the Atmospheric Sciences, 74, 699 – 717, https://doi.org/10.1175/JAS-D-16-0074.1, 2017.

Vali, G., DeMott, P. J., Möhler, O., and Whale, T. F.: Technical Note: A proposal for ice nucleation terminology, Atmospheric Chemistry and Physics, 15, 10 263–10 270, https://doi.org/10.5194/acp-15-10263-2015, 2015.

Weisman, M. L. and Klemp, J. B.: The Dependence of Numerically Simulated Convective Storms on Vertical Wind Shear and Buoyancy, Monthly Weather Review, 110, 504 – 520, https://doi.org/10.1175/1520-0493(1982)110<0504:TDONSC>2.0.CO;2, 1982.

Wernli, H., Boettcher, M., Joos, H., Miltenberger, A. K., and Spichtinger, P.: A trajectory-based classification of ERA-Interim ice clouds in the region of the North Atlantic storm track, Geophysical Research Letters, 43, 6657–6664, https://doi.org/10.1002/2016GL068922, 2016.